Sensitivity of a Square Cylinder Wake to Forced Oscillations

Sushanta Dutta

P. K. Panigrahi

K. Muralidhar

Department of Mechanical Engineering,
Indian Institute of Technology Kanpur,
Kanpur 208016, India

The wake of a square cylinder at zero angle of incidence oscillating inline with the incoming stream has been experimentally studied. Measurement data are reported for Reynolds numbers of 170 and 355. The cylinder aspect ratio is set equal to 28 and a limited study at an aspect ratio of 16 has been carried out. The frequency of oscillation is varied around the Strouhal frequency of a stationary cylinder, and the amplitude of oscillation is 10–30% of the cylinder size. Spatial and temporal flow fields in the cylinder wake have been studied using particle image velocimetry and hot-wire anemometry, the former providing flow visualization images as well. A strong effect of forcing frequency is clearly seen in the near wake. With an increase in frequency, the recirculation length substantially reduces and diminishes the time-averaged drag coefficient. The time-averaged vorticity contours show that the large-scale vortices move closer to the cylinder. The rms values of velocity fluctuations increase in magnitude and cluster around the cylinder as well. The production of turbulent kinetic energy shows a similar trend as that of spanwise vorticity with the former showing greater asymmetry at both sides of the cylinder centerline. The instantaneous vorticity contours show that the length of the shear layer at separation decreases with increasing frequency. The effect of amplitude of oscillation on the flow details has been studied when the forcing frequency is kept equal to the vortex-shedding frequency of the stationary cylinder. An increase in amplitude diminishes the time-averaged drag coefficient. The peak value of rms velocity increases, and its location moves upstream. The length of the recirculation bubble decreases with amplitude. The reduction in drag coefficient with frequency and amplitude is broadly reproduced in experiments with the cylinder of lower aspect ratio. [DOI: 10.1115/1.2742736]

Keywords: square cylinder, forced inline oscillation, drag coefficient, Strouhal number, recirculation length

1 Introduction

Bluff body wakes have been extensively investigated in view of their applications to wind engineering, hydrodynamics, aerodynamics, and electronics cooling. Such wakes display characteristics that are distinct to the object shape, Reynolds number, and distance in the streamwise direction. At high Reynolds numbers, the wake structure is complex, owing to unsteadiness and turbulence. In the lower range of the Reynolds number, recent studies with a cylinder of square cross section show that the flow field along with unsteadiness is three-dimensional, even in nominally two-dimensional geometries. In many practical applications, the flow complexity can be exploited for attaining varying degrees of control.

Active flow control using riblike structures is a recent topic of research and requires understanding of the coherent flow structures. The rib can be a cylinder of square cross section. Control is implemented by using an independent external disturbance or a feedback control system resulting in cylinder oscillations. Depending on the direction of motion with respect to the main flow direction, the oscillation may be transverse or inline. Modification of the flow field can significantly reduce or enhance the intensity of the wake.

Griffin and Ramberg [1] reviewed the wake structure of a circular cylinder oscillating inline with the incident steady flow at Re=190. Vortex shedding was seen to be synchronized with the oscillation of the cylinder in a range of frequencies near twice the shedding frequency. In one experiment, two vortices of opposite sign were shed for one cycle of cylinder motion. In another, one vortex was shed for each cycle of oscillation. Ongoren and Rockwell [2] studied near-wake flow structures arising from a transversely oscillating cylinder over a Reynolds number range of 584–1300 with the hydrogen bubble technique. The authors studied three different geometries (circular, triangular, and square) over a wide range of frequencies from subharmonic to superharmonic. The study showed a distinct phase relationship between body motion and vortex shedding for the three harmonic ranges. Roussopoulos [3] studied feedback control of vortex shedding for flow past a circular cylinder at an intermediate Reynolds number using flow visualization and hot-wire techniques. A loudspeaker was used as an actuator and the hot-wire sensor as the control. Vortex suppression was not possible if the control sensor was located too far downstream of the cylinder, even when the sensor could clearly detect the shedding. Also, suppression was not possible if the feedback loop was highly tuned to the shedding frequency. Gu et al. [4] studied, numerically and experimentally, the timing of vortex formation for a transversely oscillating circular cylinder. With an increase in the excitation frequency, the vortices were seen to move closer to the cylinder until a limiting position was reached and the vortices switched to the opposite sides of the cylinder. Tao et al. [5] reported a feedback experiment with a hot-wire probe, wherein visualization was conducted using a dye-injection technique for flow past a circular cylinder. The flow visualization images clearly showed complete vortex suppression and enhancement for various feedback conditions. Krishnamoorthy et al. [6] studied near-wake phenomena behind a transversely oscillating circular cylinder in the Reynolds number range of 1250–1500. While keeping the amplitude of cylinder oscillation fixed, the frequency of oscillation was varied. At the lower excitation frequency in the lock-in regime, the authors observed two pairs of vortices shed from the cylinder per cycle of cylinder oscillation. When the critical excitation frequency crossed the lock-in regime, one pair of vortices was shed from the cylinder.

Contributed by the Fluids Engineering Division of ASME for publication in the JOURNAL OF FLUIDS ENGINEERING. Manuscript received July 18, 2006; final manuscript received January 19, 2007. Assoc. Editor: James A. Liburdy.

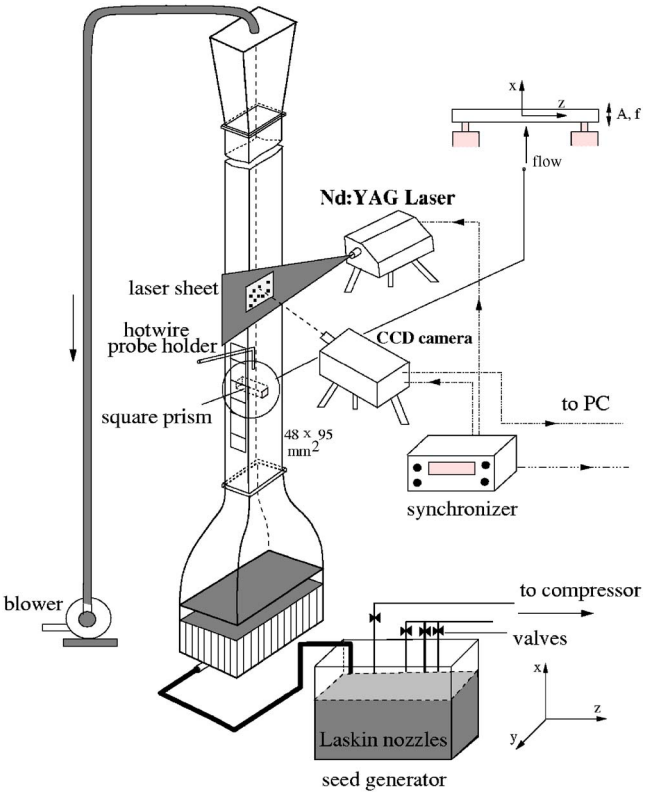

Fig. 1 Schematic drawing of the experimental apparatus

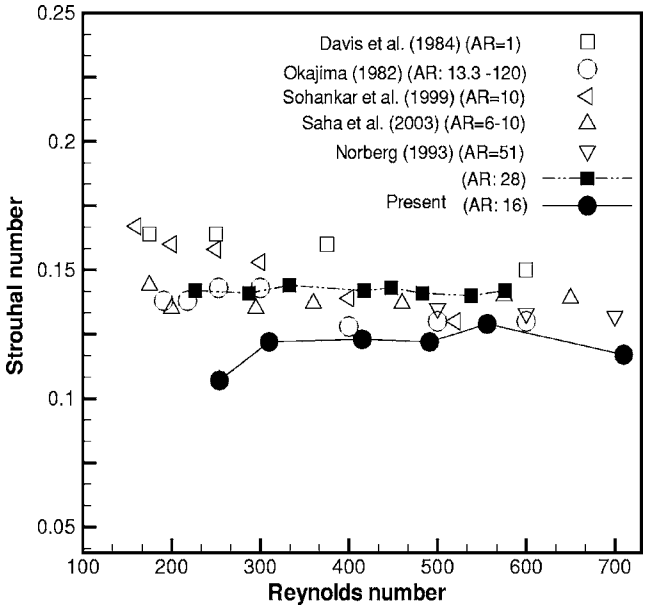

Fig. 2 Validation in terms of Strouhal number as a function of Reynolds number for flow past a square cylinder at zero angle of incidence

Cetiner and Rockwell [7] studied lock-in phenomena and dynamic loading of a circular cylinder for streamwise forced oscillations with respect to the mean flow direction over a wide range of Reynolds number ($405 < \mathrm{Re} < 2482$). Particle image velocimetry was used for the study. The authors correlated the vortex pattern with the force coefficients. The authors showed that the lock-in phenomenon is possible for streamwise oscillations because it is in transverse oscillations of the cylinder. Sarpkaya [8] reviewed vortex-induced oscillations of circular cylinders and categorized fundamental aspects of the wake behavior. Yang et al. [9] numerically studied flow past a transversely oscillating rectangular cylinder in channel flow. The authors captured flow details at a Reynolds number of 500. It was concluded that the wake pattern is dominated by the oscillations of the cylinder. Nobari et al. [10] reported numerical simulation results for flow past an oscillating circular cylinder for Reynolds numbers up to 300. Both transverse and inline oscillations were studied for various frequencies and amplitudes. The effect of the oscillation parameters on the time-averaged drag coefficient was discussed. The authors compared the results of their numerical simulations to experimental data and found a good match. Nishihara et al. [11] studied the effect of streamwise oscillation on wake pattern and fluid dynamic forces of a circular cylinder in a water tunnel using laser Doppler veloci-

Table 1 Comparison of the time-averaged drag coefficient with the published literature for flow past a stationary square cylinder

Authors	Nature of study	Aspect ratio	Blockage	Re	C_D
Davis and Moore [18]	Numerical (2D)	—	0.170	470	1.95
Sohankar et al. [19]	Numerical (3D)	6	0.055	400	1.67
Saha et al. [20]	Numerical (3D)	6–10	0.100	400	2.21
Present	Experimental	16	0.030	410	2.32
		28	0.060	420	2.03

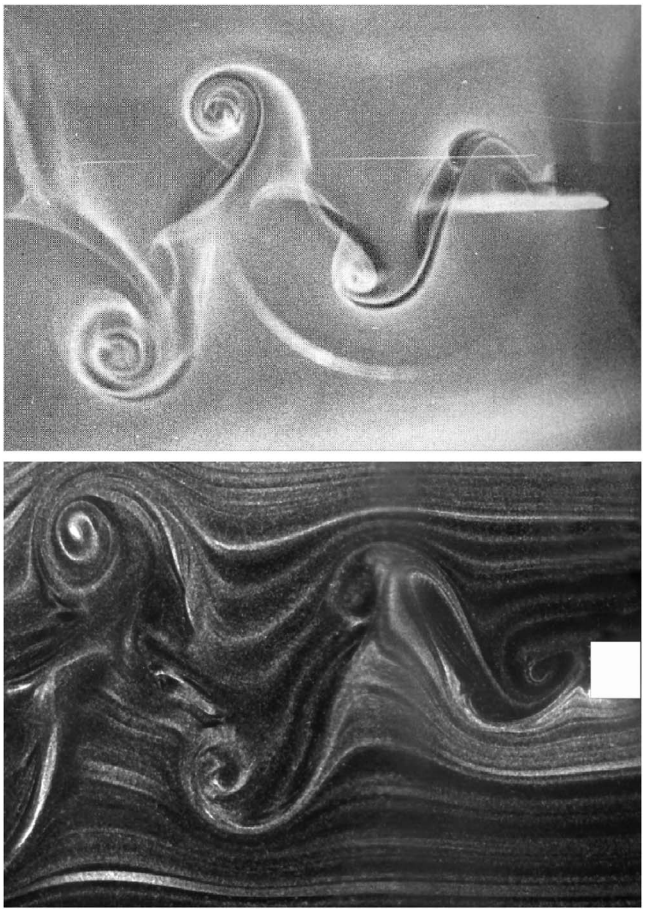

Fig. 3 Flow visualization images for inline oscillations of a square cylinder ($f/f_0=2$, below) with a circular cylinder (above) as reported by Griffin and Ramberg [1]

Table 2 Drag coefficient as a function of forcing frequency. Values outside brackets indicate momentum deficit; values within brackets include the contribution of velocity fluctuations on the time-averaged drag

f/f_o	Re=170	Re=355
0	1.48 (1.94)	1.41 (1.86)
0.5	1.13 (1.62)	0.78 (1.15)
1.0	0.94 (1.42)	0.83 (1.09)
2.0	1.05 (1.47)	0.58 (0.79)

metry (LDV) and flow visualization. The authors identified two ranges of the reduced velocity where distinct flow phenomena are observed. In the lower range ($V_r < 2.5$) symmetric vortex shedding was to be seen, whereas in the higher range ($V_r > 2.5$), alternate vortex shedding was realized.

The detailed literature review suggests that the study on effect of cylinder oscillation is primarily limited to the circular cylinder. The difference between the square and circular cylinders is the uniqueness of the location of the separation point. For the former, it is fixed at the upstream corners. For a circular cylinder, flow separation depends on the Reynolds number and freestream turbulence level. In the present work, flow past a prismatic cylinder of square cross section has been considered. The motivation for studying this geometry arises from the use of square ribs for flow control. Experiments have been conducted with an oscillating cylinder in the intermediate range of Reynolds number (170 and 355). The frequency has been varied around that of vortex shedding from a stationary cylinder. The oscillation amplitude is varied above the threshold value, while keeping the frequency equal to that of vortex shedding. For the range of parameters considered, the cylinder oscillations provide small perturbation to the wake of the square cylinder. The flow field has been explored experimentally using particle image velocimetry (PIV), hot-wire anemometry (HWA), and flow visualization. The influences of frequency and amplitude on the instantaneous and time-averaged properties of the wake of the cylinder are examined. The Reynolds number and aspect ratio effect on the wake characteristics have also been reported.

2 Apparatus and Instrumentation

Experiments have been carried out in a vertical test cell made of Plexiglas with air as the working fluid (Fig. 1). The test cell has two optical windows, one for the passage of the laser sheet and the other for recording by the camera. The cross section of the test cell is 9.5×4.8 cm^2, and the overall length is 2 m. The active length of the test cell, where measurements have been carried out, is 0.3 m. A contraction ratio of 10:1 ahead of the test section has been used. Cylinders of square cross section (3 mm and 3.4 mm edge) used for the experiments are made of Plexiglas and machined for sharp edges. Therefore, the respective aspect ratios (=length/edge) in the experiments are equal to 16 and 28. Most results have been reported for an aspect ratio of 28. With reference to Fig. 1, the x-axis is vertical and aligned with the mean flow direction. The z-axis coincides with the cylinder axis, and the y-axis is perpendicular to x and z.

The flow in the test section is set up by using the suction side of a blower driven by a voltage-stabilized single-phase motor. The freestream turbulence level in the approach flow was quite small; it was found to be less than the background noise of the anemometer (<0.05%). Flow parallelism in the approach flow was better than 98% over 95% of the width of the test cell. Stable velocities in the range of 0.5–3 m/s were realized in the test cell to cover the Reynolds number range of 100–800.

Measurements of the velocity field over selected planes were carried out using a particle image velocimetry system. The PIV system comprises a double-pulsed Nd:YAG laser (New Wave Lasers, $\lambda = 532$ nm), 15 mJ/pulse, a Peltier-cooled 12 bit CCD camera (PCO Sensicam) with a frame speed of 8 Hz, a synchronizer, a frame grabber, and a dual processor PC. The CCD is an array of 1280×1024 pixels. A Nikon 50 mm manual lens was attached to the CCD camera for covering the field of interest. The field of view for PIV measurements was 40 mm $\times$ 35 mm. From an initial size of 64×64, the final interrogation size of 16×16 pixels was arrived at by an adaptive cross-correlation method [12]. A total of 5561 velocity vectors were obtained with a spatial resolution of 0.5 mm. Inconsistent velocity vectors were eliminated by local median filtering. The time-averaged and rms velocity fields were obtained by averaging a sequence of 200 velocity vector images, corresponding to total time duration of 50 s. The instantaneous flow visualization images were recorded using the PIV system itself with a reduced particle density with a laser pulse width of 25 μs and an exposure time of 4 ms. Laskin nozzles were used to produce seeding particles from corn oil.

Local time-averaged velocity and velocity fluctuations were measured using a hot-wire anemometer (DANTEC). An X-wire probe was used for measuring two components of velocity. With the square cylinder placed horizontally, the X configuration was formed in the vertical plane. The two wires of the probe were calibrated against a pitot-static tube connected to a digital manometer (Furness Controls, 19.99 mm H_2O). The anemometer output voltage was collected in a PC through a data acquisition card (National Instruments) with LABVIEW software. Flow visualization was carried out in the test cell itself using a light sheet of the pulsed Nd:YAG laser with a reduced particle density. The cylinder was oscillated by mounting it over two electromagnetic actuators (Spranktronics) located outside the sidewalls of the test section. A small gap in the text section filled with soft rubber allowed the motion of the cylinder during actuation. Oscillation amplitude was estimated under no flow conditions by directly imaging the

Table 3 Strouhal number as a function of forcing frequency

f/f_0	Re=170	Re=355
0	0.138	0.154
0.5	0.135	0.151
1.0	0.135	0.151
2.0	0.138	0.154

Table 4 Recirculation length as a function of forcing frequency. The dimension is scaled by the edge of the cylinder.

f/f_0	Re=170	Re=355
0	2.80	2.50
0.5	3.20	2.17
1.0	1.93	1.97
2.0	0.50	1.50

Table 5 Drag coefficient, Strouhal number, and the dimensionless recirculation length as a function of forcing amplitude. $f/f_o=1$, Re=170. Values outside brackets indicate momentum deficit; values within brackets include the contribution of velocity fluctuations on the time-averaged drag. The recirculation length is scaled by the edge of the cylinder.

A/B	C_D (corrected)	St	Recirculation length
0	1.48 (1.94)	0.138	2.80
0.025	1.71 (2.27)	0.138	2.43
0.1	0.94 (1.42)	0.138	1.93
0.17	0.85 (1.14)	0.138	1.52
0.26	0.81 (1.10)	0.138	1.50
0.32	1.05 (1.40)	0.138	1.10

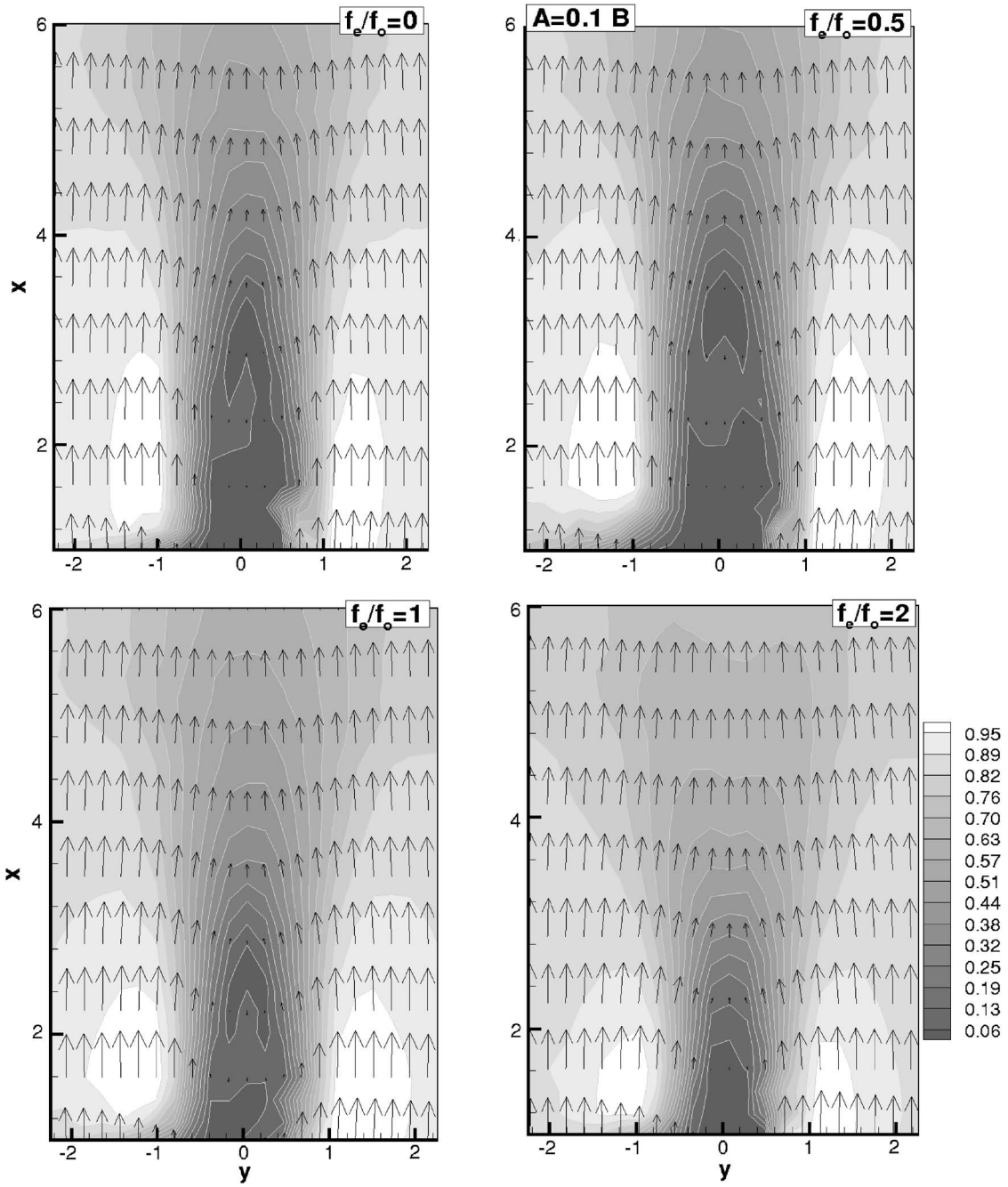

Fig. 4 Time-averaged nondimensional velocity vectors above an oscillating cylinder: Effect of frequency ratio, Re=170, *A*/*B*=0.1; flooded contours represent the absolute velocity magnitude

cylinder with the PIV camera and calibrating the pixel displacement of the cylinder with respect to the cylinder size. The actuator frequency and amplitude were adjustable through a control unit that is interfaced to a PC. The cylinders were excited at different harmonics of the shedding frequency in the streamwise direction. The amplitude of excitation was set by a voltage input to the electromagnetic actuator.

3 Uncertainty and Validation

The seeding of flow with oil particles, calibration, laser light reflection and variation in background illumination, image digitization, calculation of cross correlation, velocity gradients, and out-of-plane particle motion affect the repeatability of PIV measurements. Tracer particles need to follow the main airflow without any lag. For the particle size utilized and the range of frequencies in the wake, a slip velocity error of 0.3–0.5% relative to the instantaneous local velocity is expected. A second source of error in velocity measurement is due to the weight of the particle. In the present experiments, the effect of particle weight was examined by conducting experiments at a fixed Reynolds number by varying the size of the cylinder and air speed. The streamline plot and the dimensionless size of the recirculation region were found to be identical in each case, and independent of the fluid speed. The noise due to background light was minimized by using a bandpass filter (around the wavelength of the laser) before the camera sensor. The x- and y-component velocity profiles from PIV measurements compared very well to those from the hot wire in the far field region, confirming the proper implementation of both the

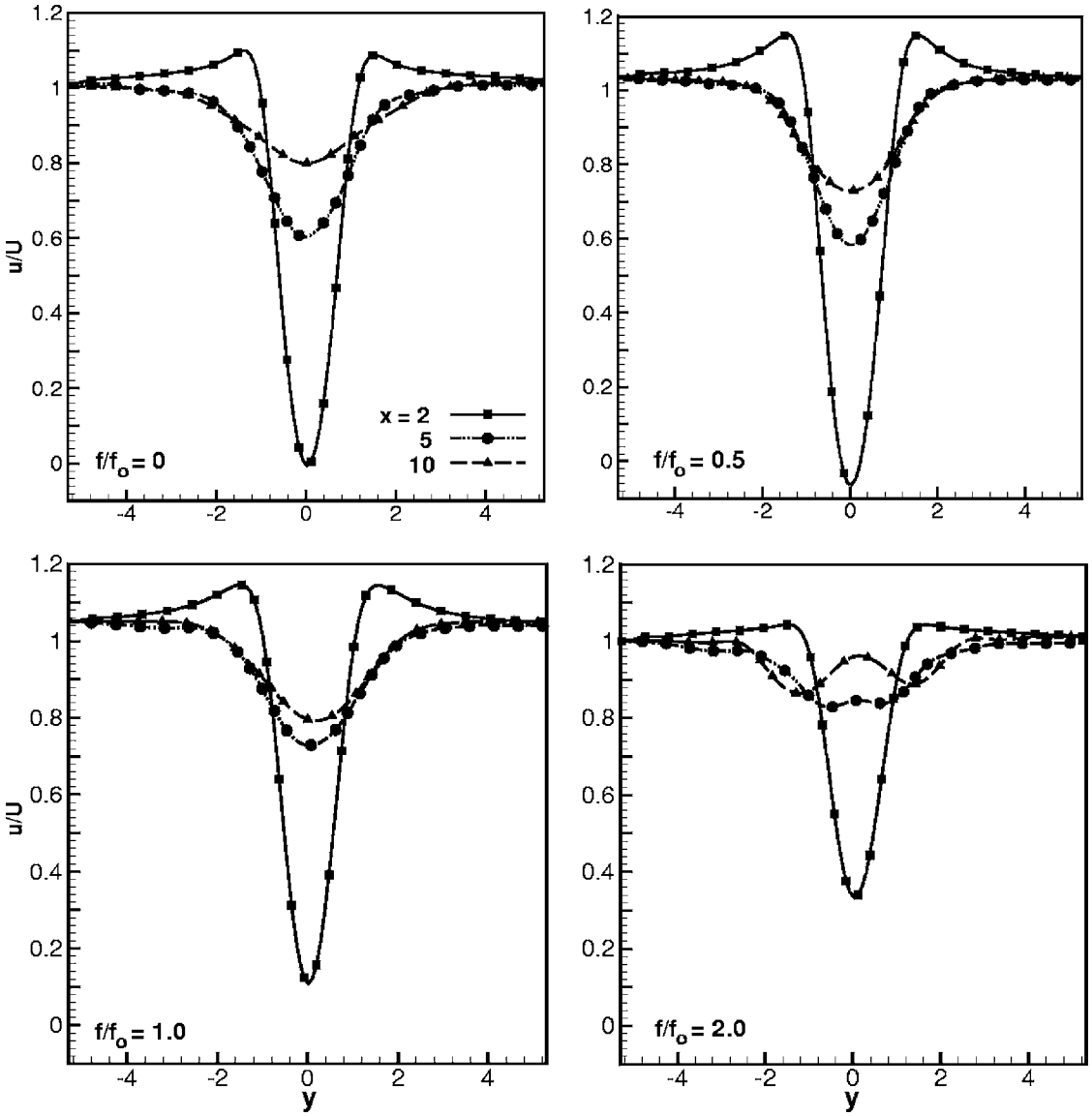

Fig. 5 Time-average *u*-velocity profiles above an oscillating cylinder at various *x*-locations: Effect of frequency ratio, Re=170, *A*/*B*=0.1

techniques and the measurement procedure. From repeated measurements (with Reynolds number kept constant to within ±1%), the uncertainty in drag coefficient was determined to be within ±5%. The uncertainty in Strouhal number was ±2%.

In experiments, the oil particle size was ~2–3 μm while the pixel size was 6.7 μm. The size of the particle image on the pixel array was estimated as 14–15 μm from a histogram distribution of light intensity over an interrogation spot. This yields a particle image-to-pixel ratio of slightly greater than 2 and fulfills the criterion recommended by Chang and Liu [13]. Other criteria, including the number of particles per interrogation spot and the average in-plane displacement discussed by Keane and Adrian [14], have also been accounted for. These criteria of particle size and number of particles per interrogation spot reduce the uncertainty in locating the peak of the cross-correlation function.

Measurements have been validated against published results for a stationary cylinder in terms of drag coefficient (Table 1), Strouhal number (Fig. 2), and visualization images (Fig. 3) in the intermediate range of Reynolds numbers. A reasonably good match of drag coefficient and Strouhal number with the literature was obtained. Figure 3 shows a comparison of flow visualization images of the square cylinder from the present work to that of the circular cylinder, as reported by Griffin and Ramberg [1]. In both experiments, the cylinders are subjected to inline oscillations at twice the Strouhal frequency. The two images show considerable similarity in terms of the wake structure.

4 Results and Discussion

The vortex formation in the near wake determines the wake structure and the forces on the cylinder. Shedding may be symmetric or asymmetric, depending on the forcing frequency. The pattern of vortex formation and the associated inline and transverse force components depend on the Keulegan-Carpenter number, $KC=2\pi A/B$, reduced velocity ($V_r=U/fB$), and velocity ratio, $U/2\pi fA$ [7,8]. Here, A is the amplitude of oscillation, B the cylinder size, and f the forcing frequency in hertz. In addition, the symbol f_0 is used for the vortex-shedding frequency of the stationary cylinder under identical experimental conditions. The present study reports results for a Keulegan-Carpenter number

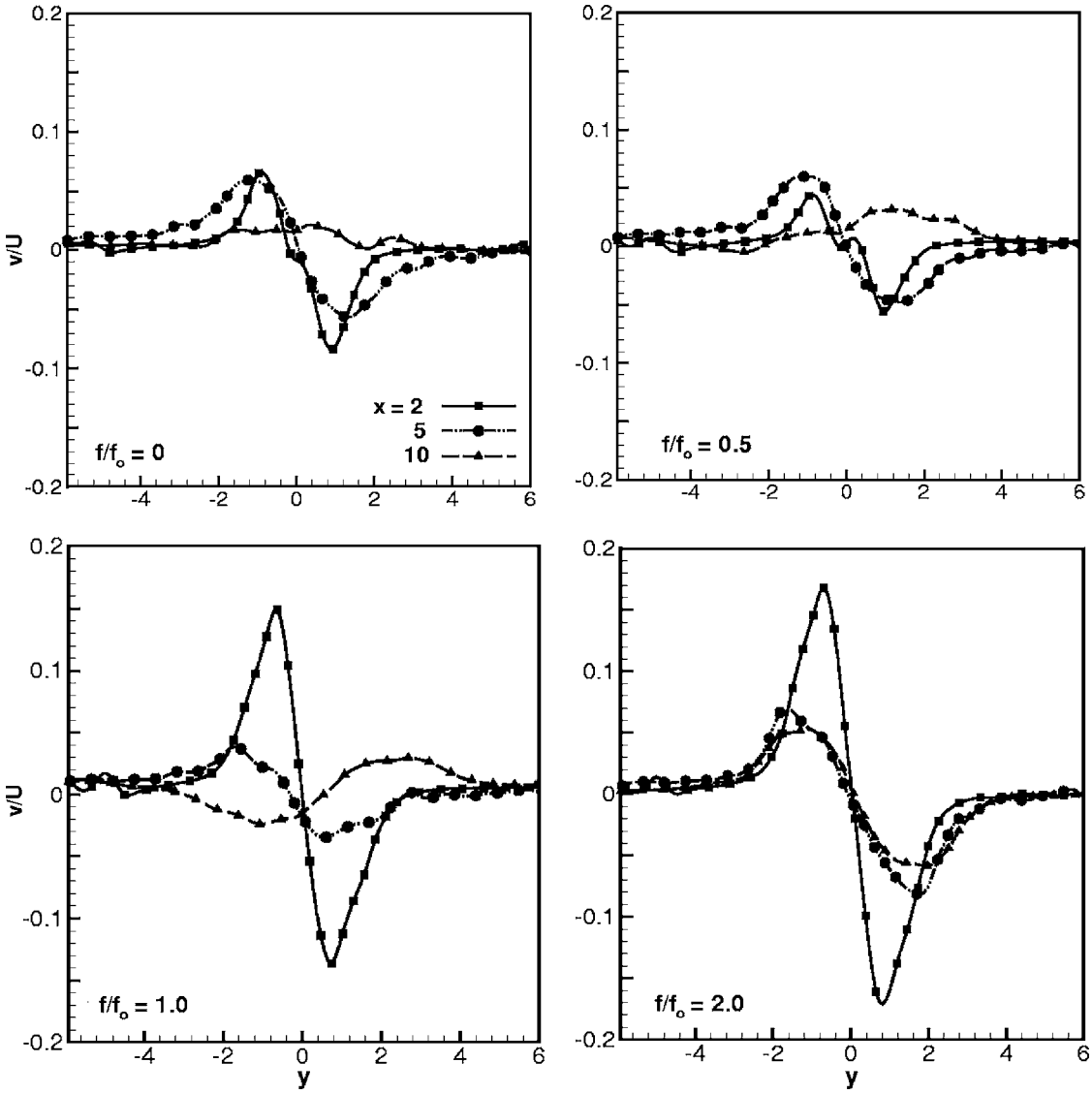

Fig. 6 Time-average *v*-velocity profiles above an oscillating cylinder at various *x*-locations: Effect of frequency ratio, Re=170, A/B=0.1

KC$<$2, reduced velocity range of 3–15, and a velocity ratio of 6–9. These parameters are such that they classify the cylinder oscillations as small perturbations to the wake.

For a stationary cylinder, the time-averaged flow field is symmetric about the x-z plane (the plane that carries the cylinder axis). Symmetry of this type breaks down for an oscillating cylinder. This is because the edge shedding a vortex and moving in the streamwise direction would produce a longer shear layer, when measured from the mean cylinder position. In contrast, an edge shedding a vortex but moving in a direction opposed to the main flow would produce a shorter shear layer. The contributions of fluid acceleration to shear layer instability at these time instants are also in opposite directions. The related asymmetry is expected to be small for small oscillation amplitudes. Asymmetry is expected to increase with the amplitude of oscillation.

The term "lock-on" is used to convey the idea that body motion is synchronized with the cycle of vortex shedding. The vortex-shedding frequency is then equal to the forcing frequency. For forcing frequencies well below lock-on, one can expect the shedding frequency to be close to the Strouhal frequency. The results presented below show that nonlinear interactions result in the appearance of additional harmonics in the power spectra.

The present work considers two Reynolds numbers (Re=170 and 355) and various amplitudes of oscillation and frequency. The frequency of oscillations is varied near the vortex-shedding frequency (f/f_0=0.5, 1, and 2) and amplitude (A/B) varied from 0.05 to 0.3. Here, the threshold amplitude of oscillation (namely, A/B=0.05) below which the wake remains unaffected is taken into account [1]. Results have been presented mainly for a cylinder aspect ratio of 28. The effect of decreasing the aspect ratio to 16 is briefly discussed.

4.1 Drag Coefficient and Strouhal Number. The drag coefficient reported here arises from the combined effect of momentum deficit and time-averaged turbulent stresses at the outflow plane of the wake. It has been determined as a time-averaged quantity from a PIV data set of 200 images. Factors such as added mass are not included in the calculation. The drag coefficient has been determined from the profiles of velocity and velocity fluctuations across the entire test cell at a streamwise location of x =10. Farther downstream (x=15), the time-averaged velocity field was significantly distorted by the presence of the wall and was not preferred. Since the plane x=10 is not sufficiently far away from

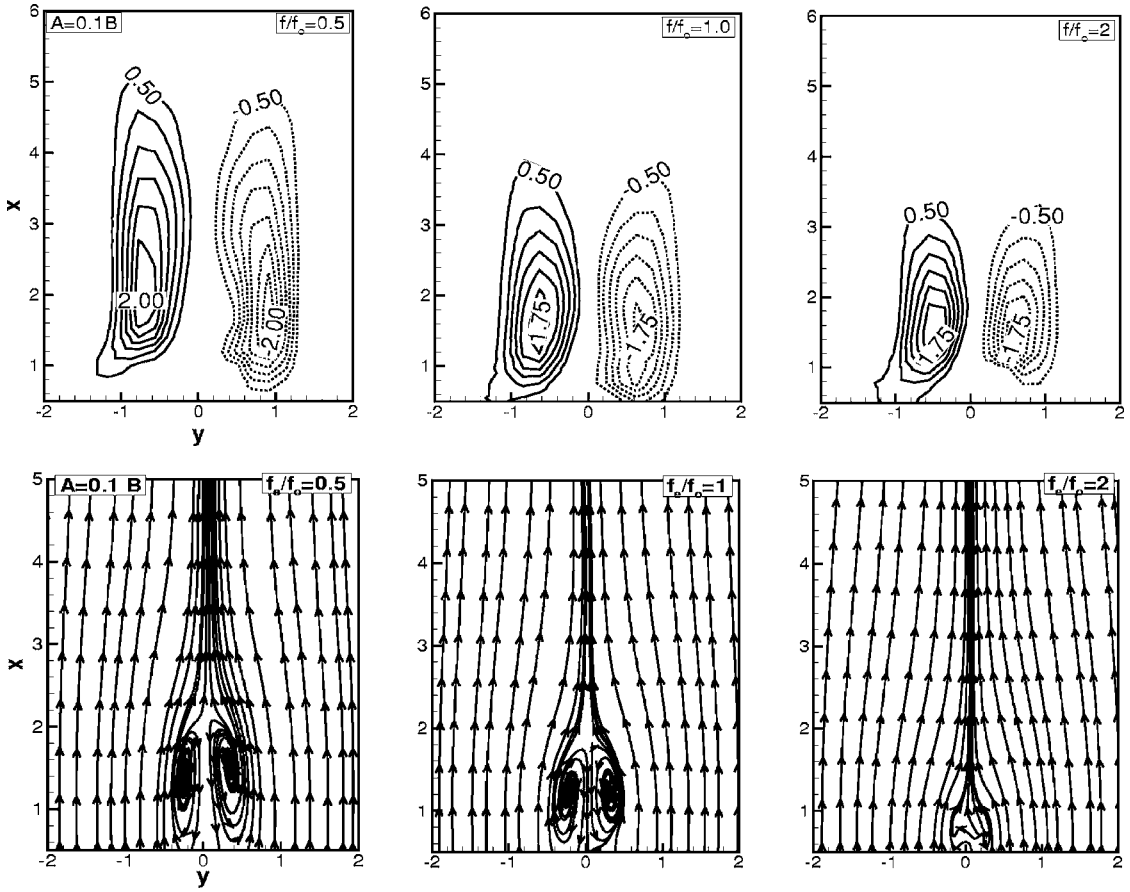

Fig. 7 Time-averaged spanwise vorticity field (top) and streamlines (below) in the wake of an oscillating square cylinder as a function of the forcing frequency, Re=170, $A/B=0.1$

the cylinder, the correction arising from turbulent stresses is expected to be significant. The drag coefficient has been calculated from the extended formula

$$C_D = 2\int_{-\infty}^{\infty} \frac{u}{U}\left(1-\frac{u}{U}\right)dy + 2\int_{-\infty}^{\infty}\left(\frac{\overline{v'^2}-\overline{u'^2}}{U^2}\right)dy$$

Here, the first term is the momentum deficit of the time-averaged flow field and the second term is the contribution of the turbulent fluctuations. The Strouhal number has been calculated from the spectral peak of the velocity trace recorded by the hot-wire anemometer.

Table 2 presents the drag coefficient measured at various frequencies of oscillation. The amplitude of oscillation is kept constant in these experiments at $A/B=0.1$. Drag coefficients have been calculated for two Reynolds numbers (Re=170 and 355). The drag coefficient decreases with respect to a stationary cylinder for an increase in the forcing frequency at both Reynolds numbers. There is a slight increase in drag coefficient when the frequency ratio increases from one to two (at Re=170), but the values are consistently smaller than for a stationary cylinder. The above trends are realized for a drag coefficient based on the momentum deficit alone as well as the total value. These results can be understood against measurements of flow patterns described in the later sections.

Table 3 presents the Strouhal number data as a function of frequency of oscillation at two Reynolds numbers (Re=170 and 355). No significant change in Strouhal number as a function of forcing frequency is observed, although its overall value increases with an increase in Reynolds number. This result is to be interpreted to mean that a significant spectral peak at the Strouhal frequency of a stationary cylinder was seen for all forcing frequencies. However, the cylinder oscillation modifies the wake structures sufficiently to reduce the momentum deficit and hence drag coefficient with respect to the stationary cylinder. Power spectra are discussed in Sec. 4.7.

The recirculation length of the time-averaged wake normalized by the edge of the cylinder in cross section is given in Table 4 as a function of frequency. This quantity diminishes with increasing frequency at both Reynolds numbers. The recirculation length scales with base pressure on the rear side of the cylinder in the sense that smaller base pressures result in longer recirculation lengths. Hence, a reduction in the recirculation length is indicative of a higher base pressure and a lower drag.

Drag coefficient and Strouhal number as functions of the amplitude of excitation are presented in Table 5. The excitation frequency is kept fixed and equal to that of vortex shedding of a stationary cylinder. A constant Strouhal number is observed with increase in amplitude of excitation indicating that the amplification of the fundamental mode is the highest among all modes and no other harmonic dominates over the basic vortex shedding process. The drag coefficient (along with the recirculation length) generally decreases with an increase in amplitude. However, when the amplitude reaches 0.32, the turbulent stresses provide a significant contribution to drag and the total drag coefficient starts to increase. The recirculation length, however, shows a continuously decreasing trend.

4.2 Velocity Field. The time-averaged velocity vectors and velocity profiles for various oscillation frequencies are shown in Figs. 4–6 for a Reynolds number of 170. Both x- and y-axes have been nondimensionalized with the cylinder size. The shaded con-

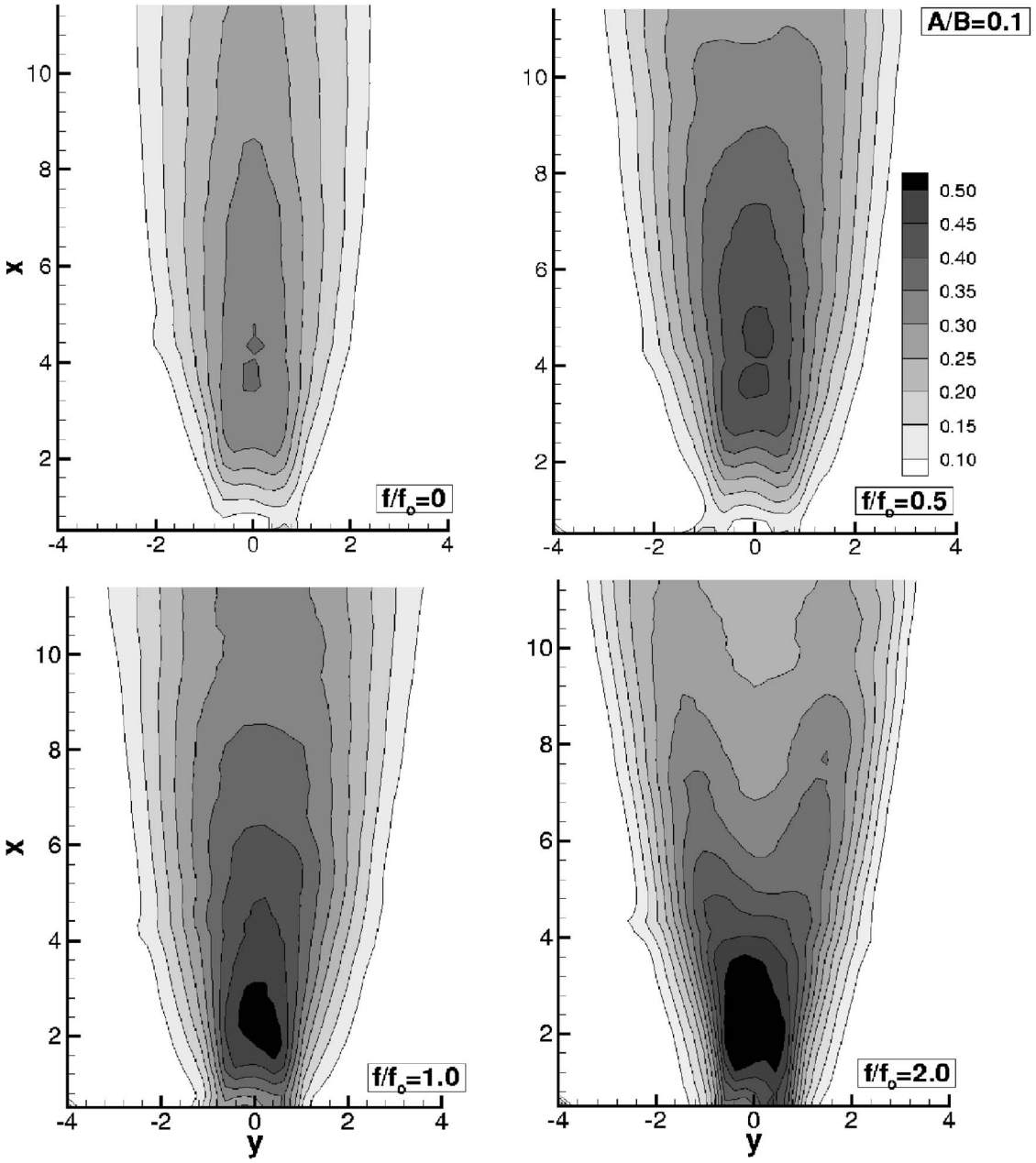

Fig. 8 Nondimensional contours of turbulent intensity in the wake of an oscillating square cylinder as a function of the forcing frequency, Re=170, A/B=0.1

tours are of resultant velocity, being the darkest in zones of small velocity magnitude. The velocity vectors in the near wake are seen to be affected by the forced oscillations. The overall shapes of the flooded velocity contours are similar for frequency ratios of 0, 0.5, and 1, but different for $f/f_0=2.0$. For this frequency ratio, the drag coefficient shows a marginal increase with respect to frequency ratio of unity (Table 2). The corresponding far-wake velocity profile shows branching in the contours and a double hump in the u-velocity profile (Fig. 5). The slight increase in drag coefficient at a frequency ratio of 2 (with respect to unity) is thus explained in terms of a broader wake that, in turn, lowers the base pressure. The origin of the broadening is explained with respect to the instantaneous plots of Sec. 4.5.

The v velocity is affected significantly by cylinder oscillations (Fig. 6). The magnitude of peak v velocity increases with an increase in the oscillation frequencies and is the highest at $f/f_o=2.0$. The overall increase in v velocity indicates greater interaction between the vortices of the neighboring shear layer. An increase in the transverse velocity with frequency is indicative of higher flow entrainment into the wake. It is, in turn, responsible for a reduction in the size of the recirculation zone (Fig. 4, also see Sec. 4.3). The shape and size of the flooded velocity contours demonstrates that the size of the recirculation zone is indeed a function of the excitation frequency. Equivalently, the magnitude of the centerline u velocity can be seen to increase in the near wake (Fig. 5).

4.3 Vorticity Field and Streamlines. Figure 7 shows the time-averaged spanwise vorticity contours for various frequency ratios (0.5, 1.0, and 2.0) at an amplitude of oscillation $A/B=0.1$. With an increase in frequency, Fig. 7 shows that the vortices, on average, move closer to the cylinder and get concentrated in the near wake. For the amplitude considered, the maximum strength of the vortices does not change significantly with the frequency of

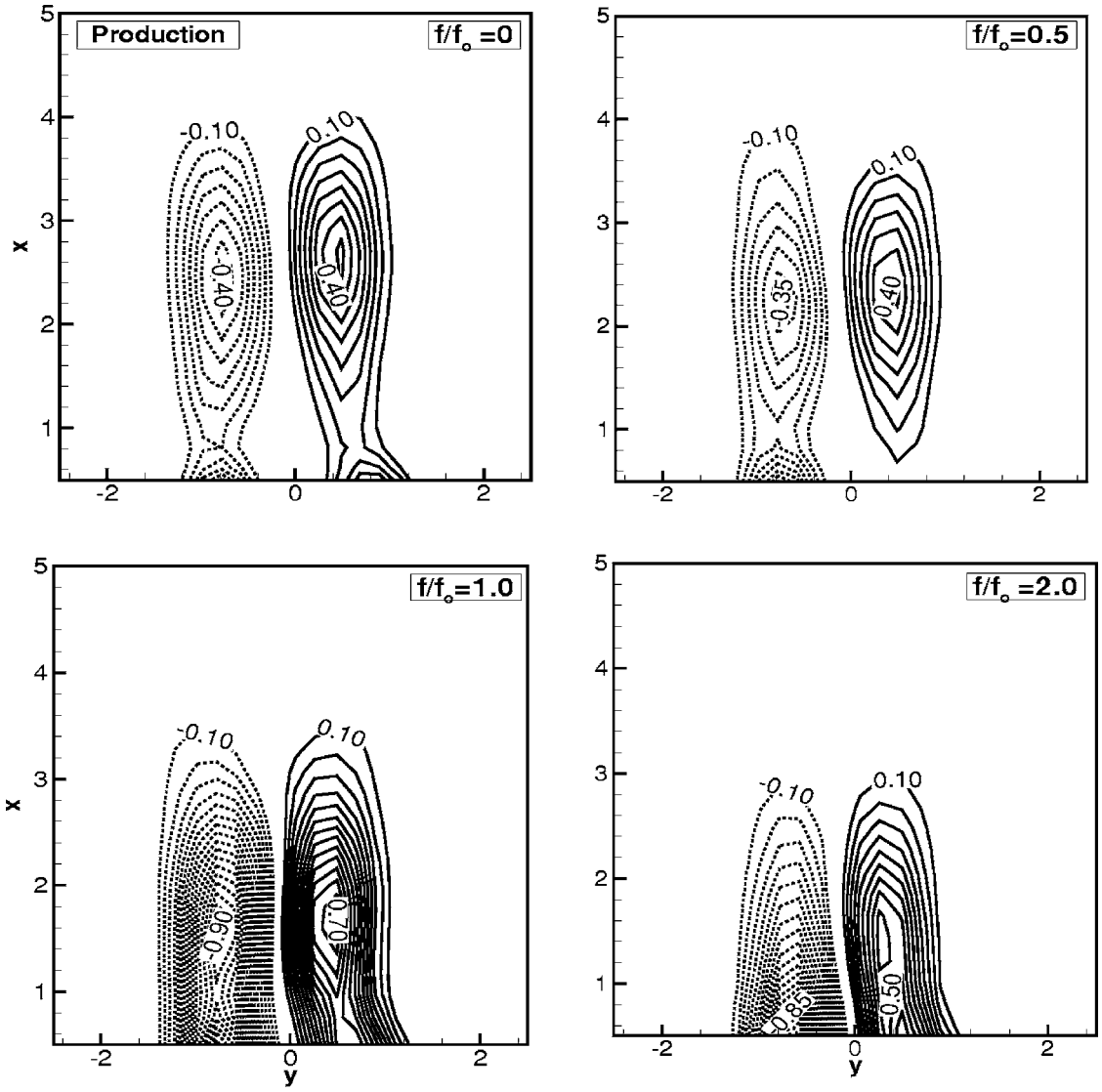

Fig. 9 Dimensionless production of turbulent kinetic energy, Re=170, A/B=0.1

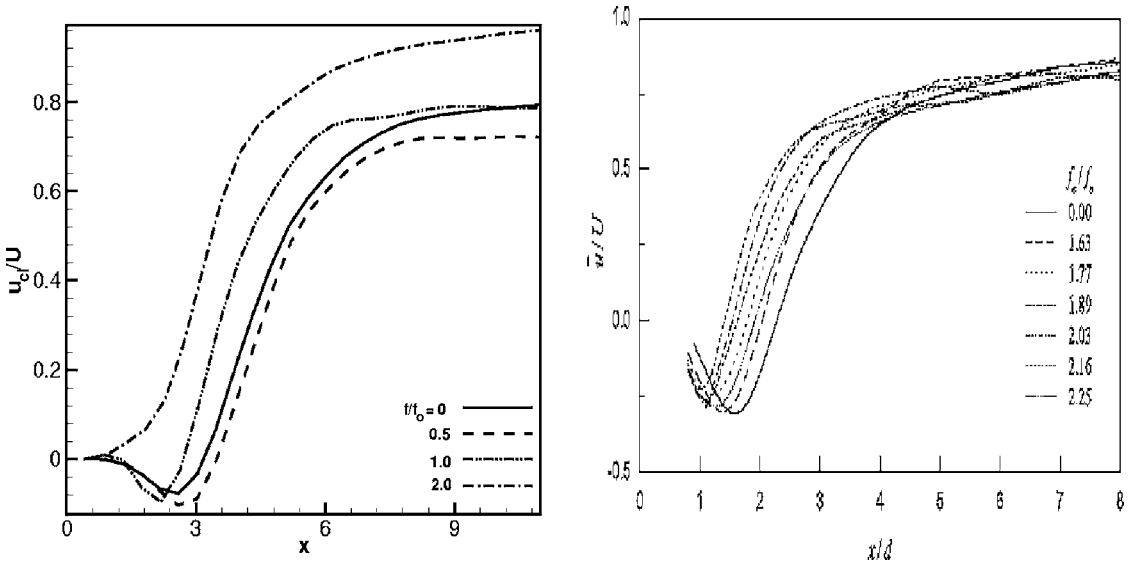

Fig. 10 Comparison of centerline recovery of streamwise velocity of the present study (left) at various oscillation frequencies with Konstantinides et al. [15] (right). The reference study is for a circular cylinder.

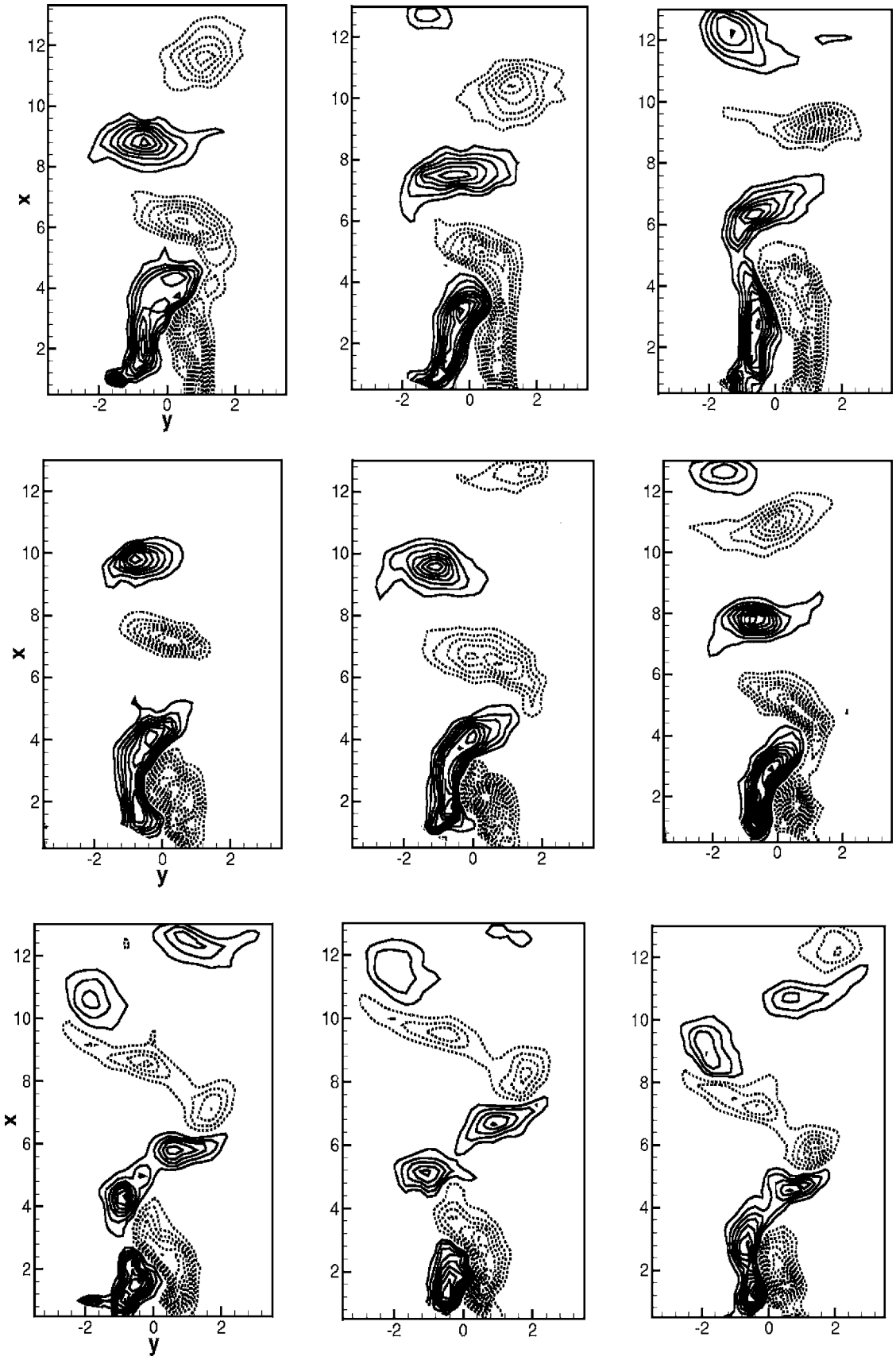

Fig. 11 Instantaneous spanwise vorticity contours above an oscillating cylinder. First row: $f/f_0=0.5$; second row: $f/f_0=1$; third row: $f/f_0=2$. $A/B=0.1$; maximum, minimum, and increments in ω_z are 3, −3, 0.25.

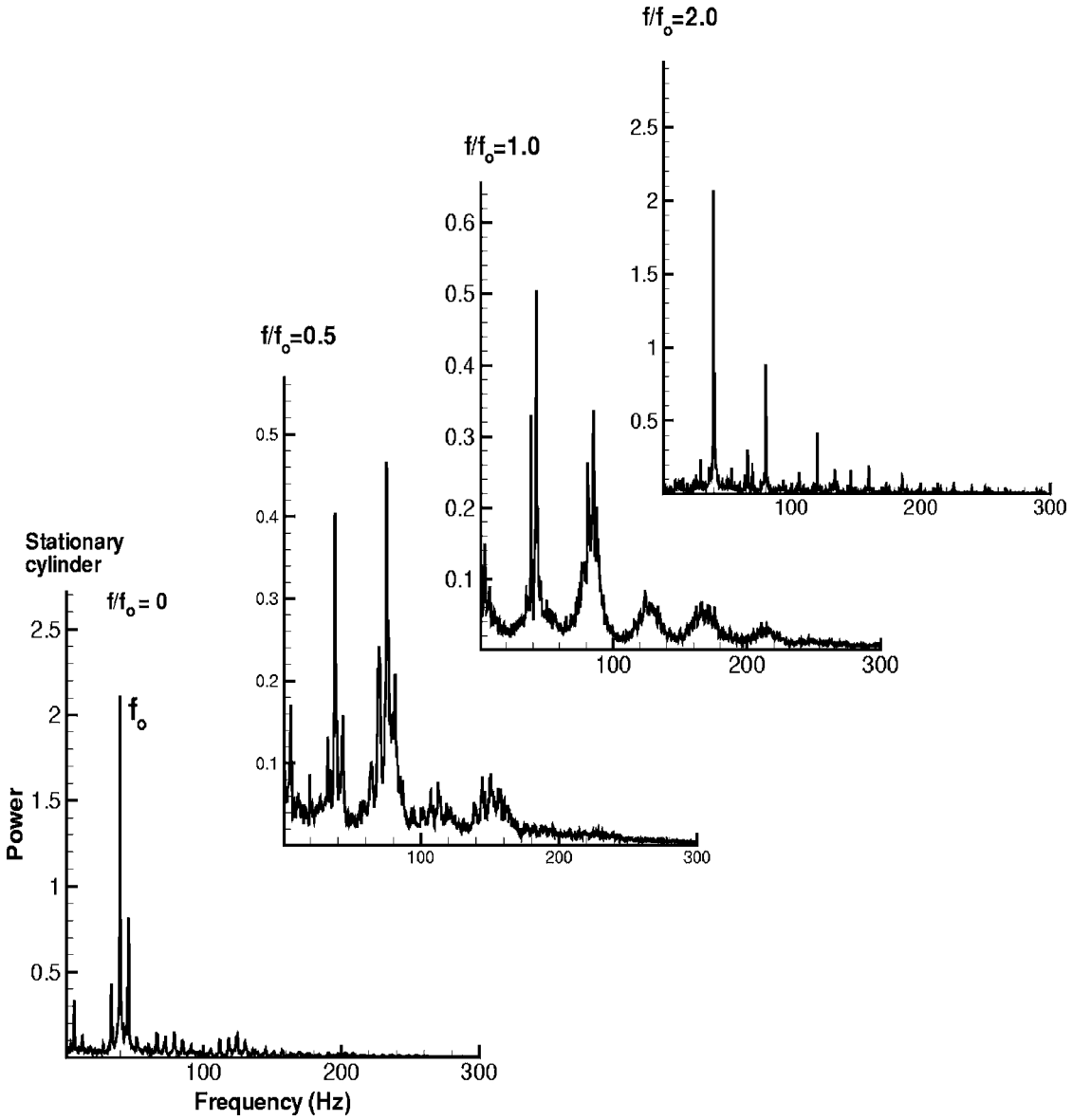

Fig. 12 Power spectra of the transverse velocity component in the wake of an oscillating cylinder; Re=170

oscillation. Vorticity concentration in the near field region has also been observed in the context of circular cylinder oscillations [4]. The movement of the point of maximum vorticity toward the cylinder confirms the reduction in the size of the recirculation zone of Fig. 4.

Vorticity in the wake can be traced to the shear layer separating at the cylinder corners. Subsequently, it is swept along the wake, while being diffused by the fluid viscosity. The vorticity production in the wake is proportional to the velocity difference between the main stream and the cylinder centerline velocity. The time instants at which flow separation takes place on each side of the cylinder correspond to distinct phases in the cylinder oscillation. Hence, the strengths of the vortices on either side of the cylinder are not necessarily of equal strength. Vortices are also subjected to strain fields imposed by the near field vortices. The vorticity contours of Fig. 7 show that for the present experiments, the effect of forced oscillations on flow symmetry is small. The sizes of two oppositely oriented vortices are close to each other and the peak values are close as well. However, the mechanism of vorticity distribution or budgets in the wake region is dependent on the excitation frequency leading to the movement of maximum vorticity zone closer to the cylinder for the excited case. The influence on the time-averaged properties, such as drag coefficient, is, however, significant (Sec. 4.1).

Figure 7 also shows the streamline contours from the time-averaged velocity vectors at the midspan of the cylinder for Re $=170$. With an increase in excitation frequency, the streamline patterns show that the size of the recirculation bubble reduces. The shape of the streamline contour is similar to that of the vorticity contours except at excitation frequency $f/f_0=2$. The size of the recirculation bubble is smaller than that of the vorticity contour. The recirculation zone for $f/f_0=2$ is smaller than the measurement zone of this study. Therefore, the recirculation bubbles are not clearly seen at $f/f_0=2$. This trend has been observed for a circular cylinder by other authors, notably Konstantinides et al. [15]. Zdravkovich [16] pointed out that wakes of a cylinder forced to oscillate in either the transverse or the streamwise direction share several characteristics, including reduction in vortex formation length and an increase in base pressure. The reduction in vortex formation length in the synchronization range has also been observed for a circular cylinder oscillated in the transverse

direction [6]. The reduction in vortex formation length indicates directly an increase in the base pressure and hence a reduction in the drag coefficient.

4.4 Velocity Fluctuations. Figure 8 shows the spatial distribution of percentage turbulence intensity (based on two components of velocity fluctuations) for a Reynolds number of 170. The turbulence intensity has been normalized with the incoming velocity. With an increase in frequency, the location of maximum turbulence intensity moves closer to the cylinder. There is a strong effect of forcing frequency on the turbulence intensity field. It increases with oscillation frequency and is highest at $f/f_0=2$. The size of the maximum turbulence intensity zone widens in the transverse direction, with an increase in excitation frequency. This observation is to be expected since advective transport of turbulent kinetic energy across the wake is governed by the fluctuating component of the transverse (v) velocity. A double peak in turbulence intensity appears on each side of the cylinder for $f/f_0=2$. This result was noted for the time-averaged velocity profile as well (Fig. 5). Hence, the field of velocity fluctuations is seen to relate to the distribution of the time-averaged streamwise velocity component. This indicates different vortex-shedding mechanisms for $f/f_0=2$ and have been discussed later in Secs. 4.6 and 4.8.

Figure 9 shows contours of the production term of kinetic energy of velocity fluctuations. This production term is defined as $\langle u'u'\rangle(\partial u/\partial x)+\langle v'v'\rangle(\partial v/\partial x)+\langle u'v'\rangle(\partial u/\partial y)+\langle u'v'\rangle(\partial v/\partial x)$ and is nondimensionalized by U^3/B. Regions of high production appear in regions of high rms velocity fluctuation of Fig. 8. In addition, the turbulent intensity production contour shape is similar to that of the time-averaged vorticity field (Fig. 7). However, the maximum magnitude of turbulent kinetic energy production distribution shows greater asymmetry between the two sides of the cylinder centerline compared to that of the vorticity for excitation frequency $f/f_0=1$ and 2. It may be noted that a higher v-velocity magnitude is seen at excitation frequencies of $f/f_0=1$ and 2 in Fig. 6. The higher value of turbulence production for these cylinder oscillation cases may be attributed to the greater magnitude of normal stresses.

4.5 Centerline Recovery. Figure 10 shows a comparison of recovery of centerline streamwise velocity with the data reported by Konstantinidis et al. [15] for various forcing frequencies. The trends in the two plots (for $f/f_0\geq 1$) are quite similar. With an increase in the forcing frequency, the vortex formation region, as measured by the distance over which negative streamwise velocities prevail, is seen to diminish in size.

Figure 10 shows that the centerline velocity drops to a minimum value and recovers subsequently for all excitation frequencies. The rate of recovery diminishes in the downstream direction. It is faster in the near field region and is also a function of the excitation frequency. With an increase in frequency, the recovery of centerline velocity is rapid for frequency ratios of 1 and 2. The PIV data of Fig. 4 also shows that the region of reversed flow decreases in size with an increase in excitation frequency when compared to a stationary cylinder. The centerline recovery is directly related to the wake width which, in turn, depends on entrainment at the edge of the wake. The greater v-velocity profile for cylinder oscillation at $f/f_0=1$ and 2 in Fig. 6 also confirms the greater entrainment from the mean flow. Figure 10 indicates an increase in entrainment with increasing frequency and the centerline recovery to be fastest at $f/f_0=2$ among all excitation frequencies considered.

The difference in centerline velocities in Fig. 10 for frequency ratios between 0 and 0.5 is small. This result is also brought out in Fig. 4, where the size of the recirculation zone is barely altered at $f/f_0=0.5$. In fact there is a slight increase, with the centerline velocity in Fig. 10 reaching an asymptotic value later, in comparison to a stationary cylinder. The reduction in drag coefficient at a

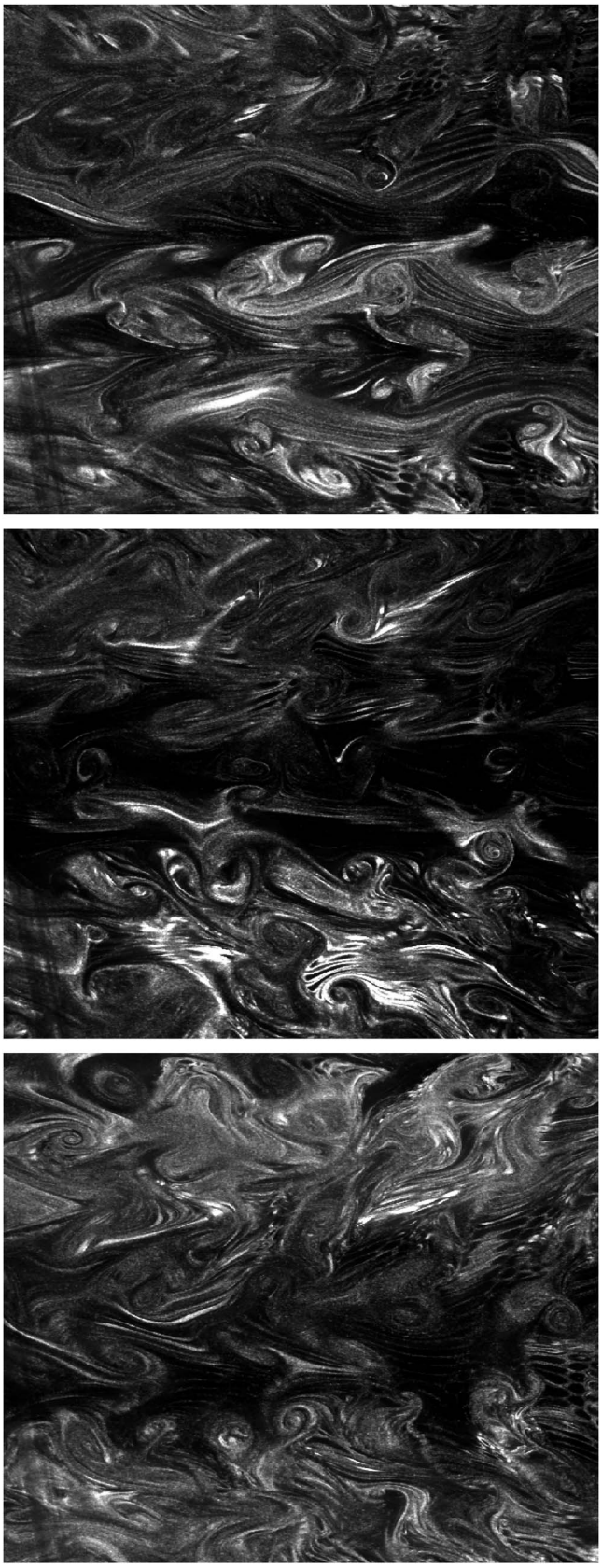

Fig. 13 Instantaneous flow visualization images on the *x-z* plane for various forcing frequencies ($f/f_0=0.5$, bottom; 1, middle; 2, top); 80% of the cylinder length is included in each frame. Main flow direction is from the right to the left.

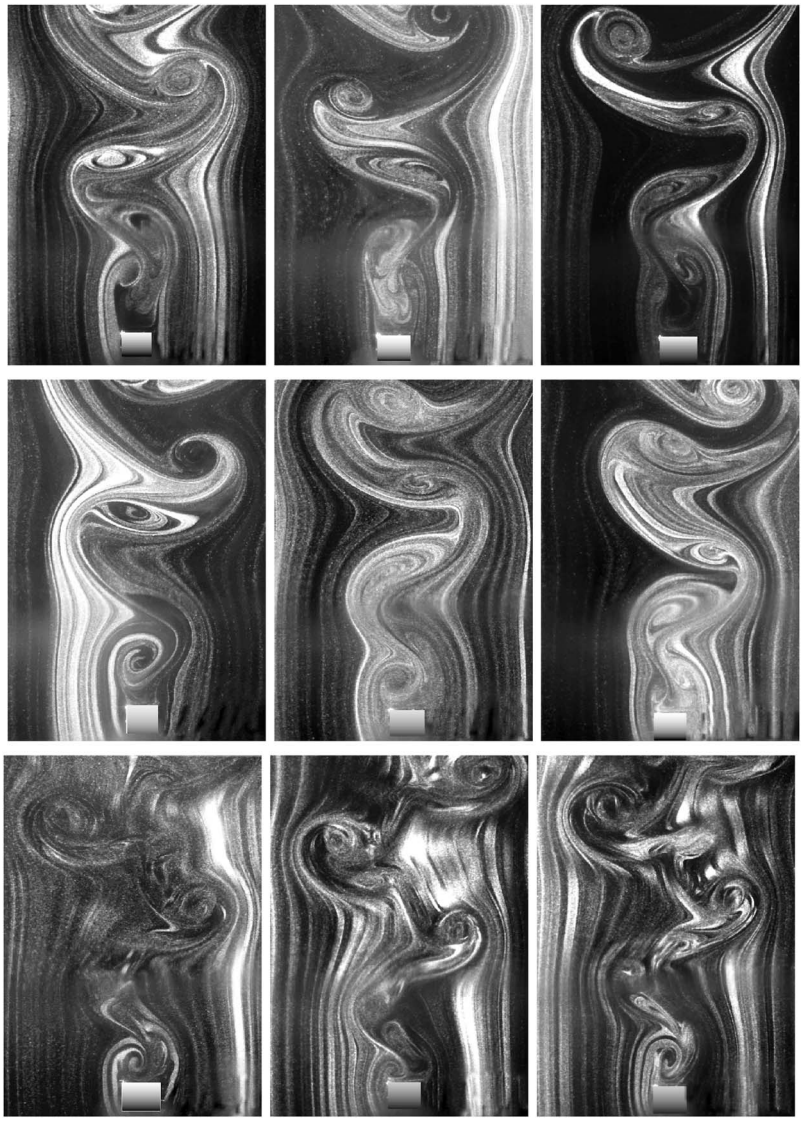

Fig. 14 Instantaneous flow visualization images in the *x-y* plane for various forcing frequencies (frequency ratios=0.5, 1, 2)

frequency ratio of 0.5 is related to the weakening of the base region though its size starts to diminish only at higher frequency ratios.

4.6 Instantaneous Spanwise Vorticity Field. Figure 11 shows instantaneous vorticity contours at selected instants of time for different frequencies of oscillation. As the frequency increases, the near-wake vortex pattern changes due to a change in the characteristics of vortex shedding. The vortices grow behind the cylinder and are subsequently shed. The vortex roll-up distance decreases with an increase in frequency. The vortex roll-up distance is the lowest at the highest excitation frequency ($f/f_0=2$). The reduction in the streamwise length scale carries over to the time-averaged data as well (Fig. 7). The alternate vortices shed from the cylinder are transported in the downstream direction. The vortex shed from one shear layer is drawn toward the other. This process repeats for both sides of the shear layer. The lateral movement of the vortices is the highest for an excitation of $f/f_0=2$. At this frequency of excitation, two neighboring vortices travel as a group having smaller streamwise separation compared to the subsequent pair of vortices. The dual peak in the streamwise velocity profile (Fig. 5) and that in the turbulence intensity distribution of Fig. 8 can be attributed to the higher lateral movement of the separated shear layers at $f/f_0=2$. The large spread of vorticity in the transverse direction at a frequency ratio of 2 is also indicative of a lower base pressure and slightly higher drag (Table 2).

Alternate shedding of vortices, typical of a stationary cylinder, is referred to as the *S* mode in the literature [8]. The lateral (transverse) movement of vortices is the *P* mode and is observed for transverse oscillation of the cylinder with respect to the mean flow direction, Williamson and Roshko [17]. In the present experiments, the shedding pattern is seen to be predominantly of the *S* type. At the frequency ratio $f/f_0=2$, a combination of *P* and *S* modes is observed.

4.7 Power Spectra. Figure 12 shows power spectra at a Reynolds number of 170 for three nondimensional forcing frequencies along with the stationary cylinder. The spectra were obtained from a long-time signal of 20,000 samples at a sampling rate of 1000 Hz. Spectra have been calculated based on the v component of velocity (at $x/B=5$ and $y/B=1$) and normalized by their respective areas under the curve. The time record involves at least 300 cycles of vortex shedding. For the low Reynolds number experiment (Re=170), a pure Karman vortex shedding pattern is observed for a stationary cylinder. It corresponds to a single

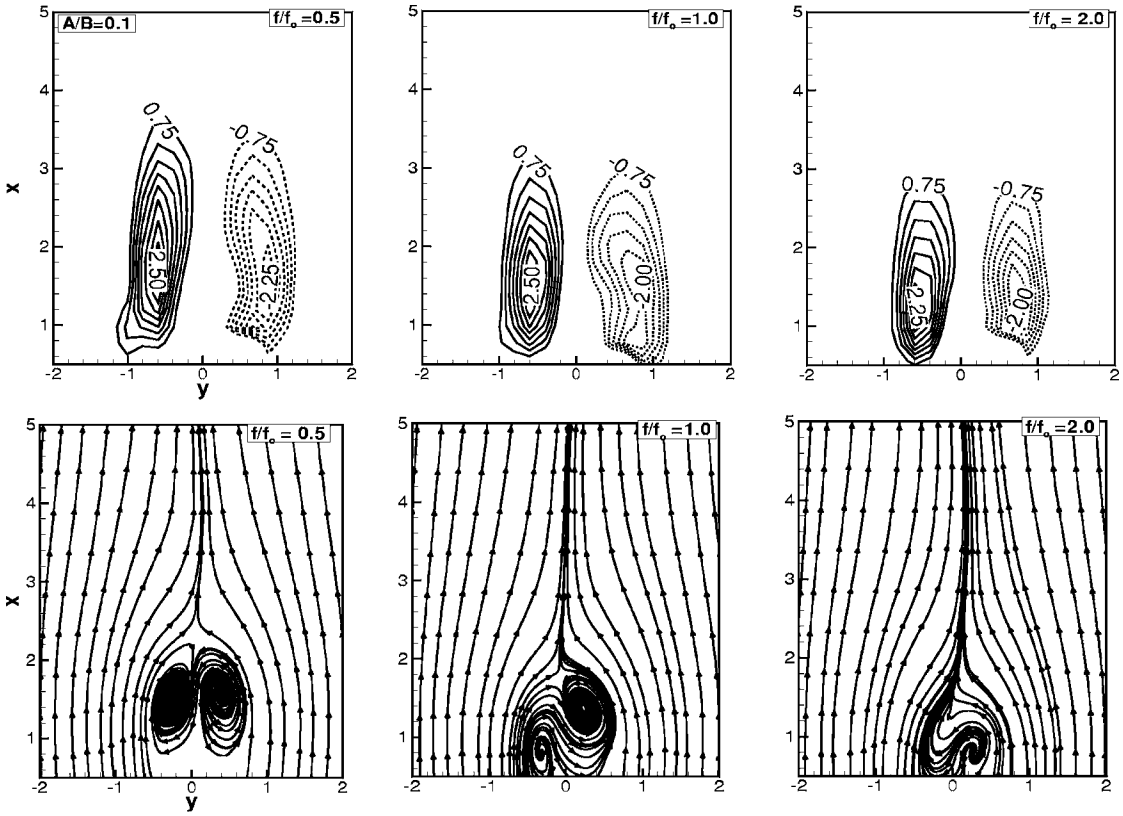

Fig. 15 Time-averaged spanwise vorticity contours (ω_z) and streamlines in the wake of a square cylinder at various frequency ratios (0.5,1,2) with a perturbation amplitude at A/B=0.1 and Re=355

sharply defined peak of vortex shedding in the spectra (at 39 Hz). With externally applied forcing frequency, Fig. 12 shows that a spectral peak is consistently seen at 39 Hz, though additional spectral peaks appear in the spectra. At a forcing frequency ratio of 0.5, the unsteadiness due to cylinder motion at a frequency of 19.5 Hz is not to be seen. Instead, a peak at 78 Hz higher than the one at 39 Hz is realized. The excitation at subharmonic frequency (f/f_0=0.5) has been observed to contribute toward vortex merging in the mixing layer. The absence of a spectral peak at f/f_0 =0.5 for square cylinder oscillation indicates absence of vortex merging phenomena due to subharmonic excitation. At a frequency ratio of unity, the cylinder motion reinforces vortex shedding and the peak shifts clearly to 39 Hz. The nonlinear interaction between the forcing signal and vortex-shedding frequency generates sum and difference frequencies in the spectrum and is responsible for the second peak. At a frequency ratio of 2, the peak remains at 39 Hz and its magnitude is significantly greater than at 0.5 and unity. An additional smaller peak corresponding to cylinder motion is seen at 78 Hz. The increase in the magnitude of the spectral peak to a value close to that of the stationary cylinder shows that lock-on conditions prevail in the wake. This is consistent with the data of Griffin and Ramberg [1], who show that lock-on should appear for an amplitude ratio of 0.1 and a frequency ratio of 2, but not for other frequency ratios. The authors also suggest that the flow field would be close to two-dimensional under lock-on conditions. This conjecture is supported by the flow visualization images of Fig. 13. Here, the particle traces tend to get straightened at the highest frequency ratio (f/f_0=2).

4.8 Flow Visualization Images. Figure 14 shows particle traces in the cylinder wake recorded using PIV at forcing frequencies of 0.5 (first row), 1 (second), and 2 (third). The first column corresponds to the instant when the cylinder is at its extreme top position. The second has the cylinder at the mean position, while the third column corresponds to the lowest position of the cylinder. The flow distribution for a stationary cylinder, namely, alternate shedding of vortices from either side of the cylinder, is quite similar to that corresponding to a frequency ratio of 0.5 and is not shown. The streamwise distance over which a vortex rolls up relative to the cylinder position known as vortex formation length decreases with an increase in frequency of oscillation. The reduction in the vortex formation length carries over to the time-averaged data as well (Fig. 7). For all three frequencies, the vortex detaches from the upstream corner during the passage of the cylinder in the downward direction. The phase corresponds to the extreme top position of the cylinder. For frequencies of 0.5 and unity, the centers of vortices essentially remain on one side of the midplane. At a frequency ratio of 2, the wake reveals new features. Eddies are shed jointly from both sides of the cylinder, while alternate shedding also persists with a phase difference. The wake reveals two length scales corresponding to the separating shear layer and the spacing between vortices. The centers of the shed vortices move across the cylinder midplane. There is a broadening of the wake as well. The interaction between the neighboring vortices of the opposite shear layer is interrupted by the intermediate vortex structure appearing behind the primary large-scale shed vortex. These factors result in the double-peaked distribution of rms velocity contours (Fig. 8), slight increase in drag coefficient (Table 2), and additional harmonics in the power spectra.

4.9 Effect of Reynolds Number. Results discussed above are mainly at a Reynolds number of 170. Experiments have also been conducted at a second Reynolds number of 355. Broadly, no difference was seen in the wake behavior. The time-averaged vorticity and streamline plots at the higher Reynolds number are shown in Fig. 15. The vorticity plots look similar to Fig. 7 at Re=170, though the peak vorticity at the higher Reynolds number is also

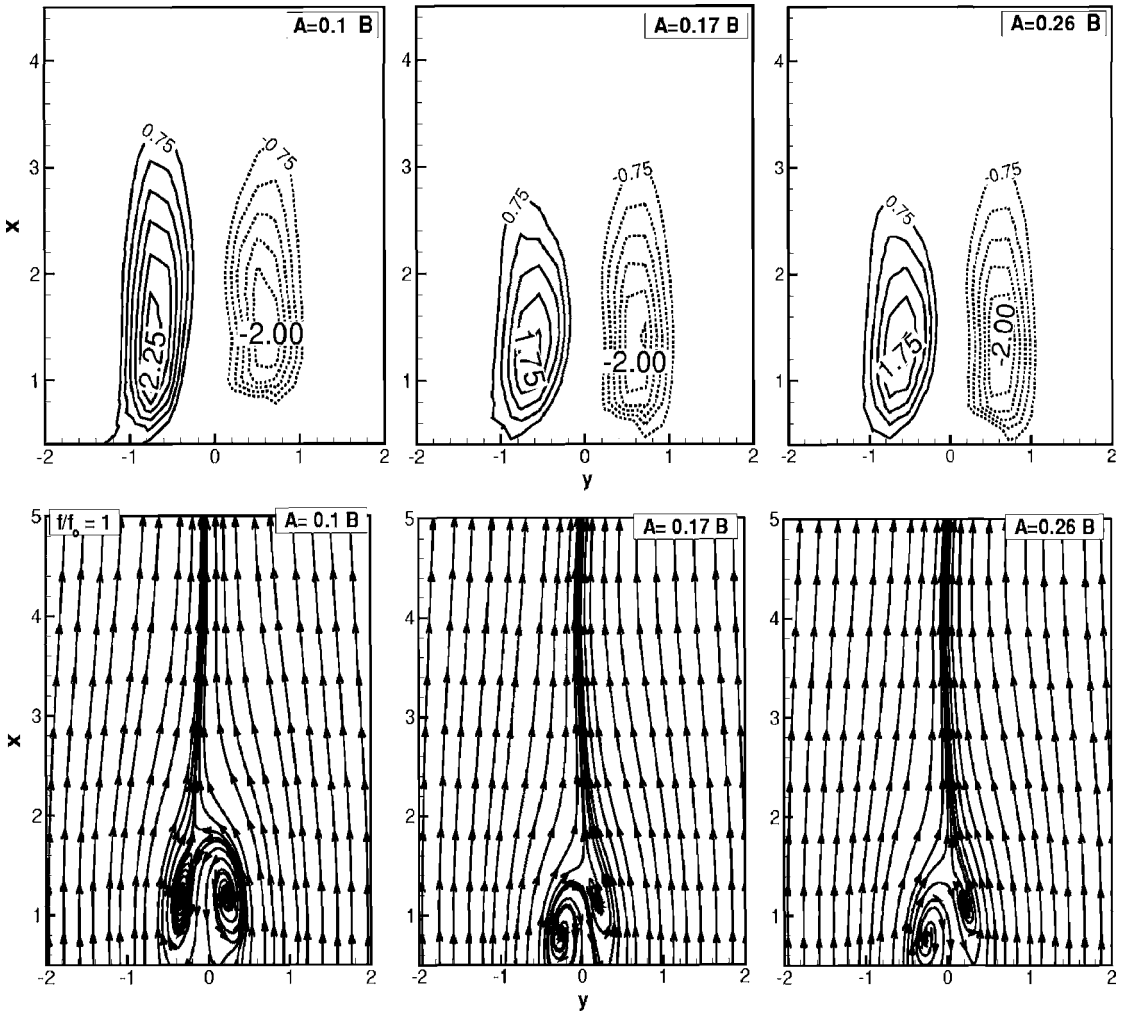

Fig. 16 Time-averaged vorticity and stream traces for various amplitudes of oscillation (A/B=0.1,0.17,0.26) at a forcing frequency f/f_0=1, Re=170

higher. To a first approximation, one can surmise that the effects of Reynolds number and frequency on the wake are independent. The effect of forced oscillations on flow symmetry is marginal, as seen from vorticity contours. The sizes of two oppositely oriented vortices are similar to each other, though not equal for the frequencies considered. The length of the recirculation bubble decreases with an increase in forcing frequency as in the lower Reynolds number experiments (Re=170). The streamline plots indicate greater asymmetry between the recirculation bubbles at the opposite sides of the cylinder centerline for excitation at f/f_0=1 and 2. The vortex formation length at both sides of the cylinder is affected to a greater extent for higher Reynolds number leading to greater asymmetry in flow structures at both sides of the cylinder.

4.10 Effect of Amplitude. In the present section, the effect of amplitude of oscillation on the flow structures is discussed. The forcing frequency is kept equal to the vortex-shedding frequency. With an increase in amplitude, the momentum flux pumped into the near wake of the cylinder increases. The vortex formation length reduces with an increase in the amplitude. These changes in the near-wake vortex formation process cause corresponding changes in the strength of the shed vortices. The increase in vortex strength can be interpreted as a corresponding increase in the rate of vorticity generation.

Time-averaged drag coefficient, Strouhal number, and recirculation length as functions of the amplitude of excitation are presented in Table 5. A constant Strouhal number is observed at all excitation amplitudes, indicating that the amplification of the fundamental mode is highest among all other modes and no other harmonics dominates over the vortex shedding with an increase in amplitude of excitation.

The time-averaged spanwise vorticity contours for various oscillation amplitudes are shown in Fig. 16. The time-averaged vorticity contour size reduces with increase in excitation amplitude, and the average vortex structure moves upstream toward the cylinder. An upstream migration of the large-scale vortex structure has also been observed earlier by Ongoren and Rockwell [2] for transverse oscillation experiments with cylinders of circular, square, and triangle cross sections.

Figure 16 also shows the streamline plot derived from the time-averaged velocity field. The size of the recirculation zone reduces with an increase in the amplitude of oscillation. When compared to the effect of forcing frequency on recirculation length, the effect of amplitude is less prominent. Simultaneously, an asymmetry in the flow field starts to appear. The increase in amplitude of oscillation makes the flow field asymmetric due to a distortion in the phase relationship between cylinder movement and the vortex shedding cycle. A strong coupling between oppositely oriented vortices is responsible for the asymmetry in the time-averaged data.

The effect of oscillation amplitude on the flow field can be understood from the following idealized context. Consider a situation where a cylinder moves in an infinite fluid and the superim-

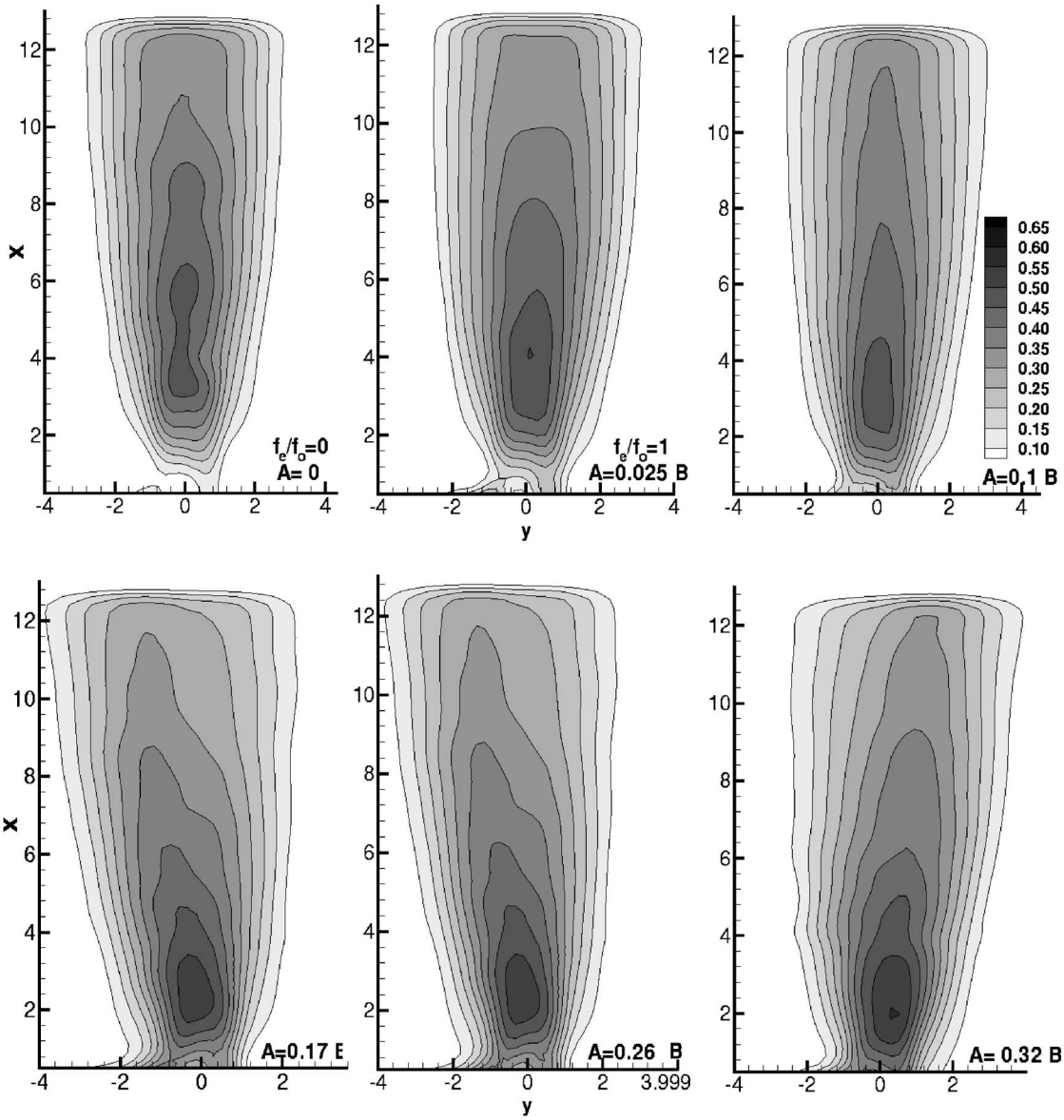

Fig. 17 Rms contours for various amplitudes of oscillation, Re=170

posed flow is zero. For a square cylinder with inline oscillations, two fixed stagnation points at the front and back of the cylinder are available. The resulting vortex-generation process can be described as follows. As the oscillating cylinder moves in the forward direction, two boundary layers develop on the cylinder wall. The separating flow creates two counterrotating vortices of equal magnitude and strength, resulting in geometrically similar vortex fields. The creation of vortices stops when the maximum forward location of the cylinder is reached and the cylinder starts its backward motion.

The vortex formation process is now repeated on the other side of the cylinder. In addition, the backward motion of the cylinder causes a splitting of the vortex pair, produced earlier by the forward motion, until, finally, flow reversal occurs. Thus, cylinder oscillation creates a strong damping effect in the near flow field and a concentration of vortices in the near wake of the cylinder. The higher the amplitude of oscillation is, the larger the damping effect is. One can now expect the superimposed flow to modulate the vortex-generation process described above because of vortex shedding.

Figure 17 shows the nondimensional turbulence intensity field at various amplitudes of oscillation. The turbulent intensity near the cylinder increases as more energy enters the flow field from cylinder excitation. The maximum intensity value moves toward the cylinder with an increase in excitation amplitude. The degree of asymmetry increases as well with an increase in the amplitude.

Figure 18 shows the power spectra of velocity signals in the near wake at different amplitudes of oscillation. With an increase in the amplitude of oscillation, multiple harmonics of the frequency of vortex shedding start to appear. At a particular amplitude ($A/B=0.32$), the flow field is dominated by the forcing frequency and only one dominant peak is seen in the power spectra. This may be considered as a lock-on state, and the flow can be considered increasingly two-dimensional with increase in amplitude.

4.11 Effect of Aspect Ratio. A limited study was carried out to investigate the effect of aspect ratio on the near wake of a cylinder under oscillatory conditions. While the aspect ratio considered in earlier sections was 28, the aspect ratio in the present discussion is 16. For definiteness, a Reynolds number of 170 is considered. The effects of frequency as well as amplitude of oscillation are investigated.

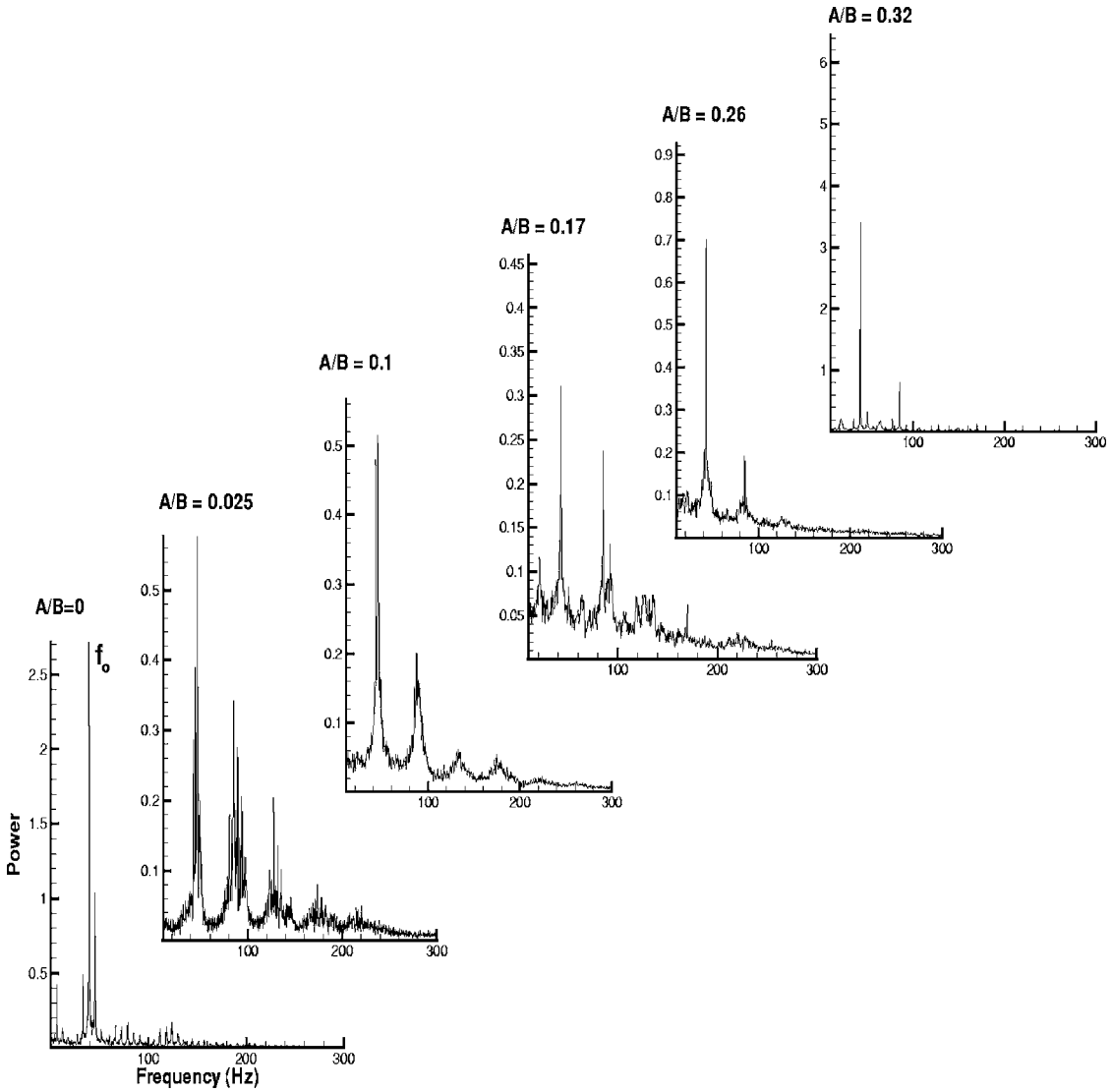

Fig. 18 Power spectra for various amplitudes of oscillation, Re=170

Table 6 summarizes the time-averaged drag coefficient data for two aspect ratios 16 and 28 for various frequencies and amplitudes of oscillation. In the study of the effect of frequency, the amplitude is kept constant at 0.1. In the second set of experiments, the forcing frequency is that of vortex shedding, while the amplitude is varied. The overall drag coefficient is lower at the higher aspect ratio for both unexcited and excited cylinders. A minimum in drag coefficient is seen for a frequency ratio $f/f_0=1.0$ for the two aspect ratios. This indicates that the end conditions due to the difference in aspect ratio do not alter the effect of cylinder oscillation. The magnitude of drag coefficient at AR=16 is uniformly higher when compared to the higher aspect ratio experiments. This effect of aspect ratio on drag coefficient was seen for a stationary cylinder as well. The drag coefficient diminishes rapidly with an increase in the amplitude of oscillation.

Figure 19 shows the time-averaged spanwise vorticity contours for various frequencies ($f/f_0=0.5$, 1.0, and 2.0) and amplitudes ($A/B=0.1$, 0.14, and 0.21) at the aspect ratio of 16. With an increase in the forcing frequency, the vortices concentrate near the rear surface of the cylinder. Similar trends were observed at the higher aspect ratio (Fig. 7). However, the strength of vorticity is higher in the lower aspect ratio experiment (Fig. 19) when compared to the higher one (Fig. 7). The higher vorticity at lower aspect ratio may be related to the confinement effects. The comparison of Fig. 19 (top) with Fig. 19 (bottom) indicates similar effects of excitation amplitude and frequency. Overall, aspect ratio does not alter the characteristics of the oscillating cylinder.

5 Conclusions

An experimental study of uniform flow past an oscillating square cylinder is reported. Measurement techniques are based on PIV, HWA, and flow visualization. The Reynolds number mainly considered is 170, while selected results for Re=355 have also been presented. The cylinder is oscillated using an electromagnetic actuator at around the vortex-shedding frequency of the equivalent stationary cylinder. The following conclusions have been arrived at in the study:

1. Effect of frequency ($A/B=0.1$; Re=170). A strong effect of forcing frequency is clearly to be seen in the near wake. The recirculation length reduces by a factor of 5 for an increase in frequency ratio from zero to two. The time-averaged drag

Table 6 Comparison of drag coefficient as a function of forcing frequency and amplitude for two aspect ratio (AR=16 and 28) at Re=170. Drag coefficients are based on the momentum deficit of the wake.

A/B	AR=16	AR=28
0	2.34	1.48
0.05	2.55	-
0.1	1.91	0.94
0.17	1.72	0.85
0.23	1.34	0.81
0.27	1.21	-
f/f_{o0}	AR=16	AR=28
0	2.34	1.48
0.5	2.61	1.13
1.0	1.91	0.94
2.0	2.02	1.05

acting on the cylinder is correspondingly lowered by ~25% from that of a stationary cylinder. The contribution of the turbulent stresses on the time-averaged drag coefficient is in the range of 30–50%, thus being significant in all experiments. The instantaneous vorticity contours show the length of the shear layer to be lowered before separation; hence, the longitudinal wavelength of the shed vortices reduces. With an increase in frequency, the large-scale vortices move closer to the cylinder. The rms velocity fluctuations cluster around the cylinder as well, though they spread in the transverse direction. Power spectra reveal lock-on conditions only at the highest frequency ratio.

2. Effect of amplitude ($f/f_0=1$; Re=170). The effect of increasing the amplitude at a given frequency leads to a reduction in the length of the recirculation bubble by ~57% of a stationary cylinder. The reduction in the time-averaged drag coefficient is ~30% when the highest amplitude ratio of 0.32. The time-averaged velocity profiles show asymmetry with increase in the perturbation amplitude. Asymmetry is related to the phase difference between the vortex-shedding mechanism and the cylinder motion. The peak value of rms velocity increases with amplitude, being 80% higher at the highest amplitude. The peak rms value also moves upstream toward the cylinder with an increase in the amplitude. Lock-on conditions were seen at the highest amplitude ratio of 0.32.
3. Effect of aspect ratio. With an increase in frequency and amplitude of oscillation, the recirculation length reduces. The time-averaged momentum deficits of the lower aspect ratio cylinder exceed those of the higher by a factor of 60%. However, the effects of forcing frequency and amplitude on the wake properties are similar at aspect ratios of 16 and 28.

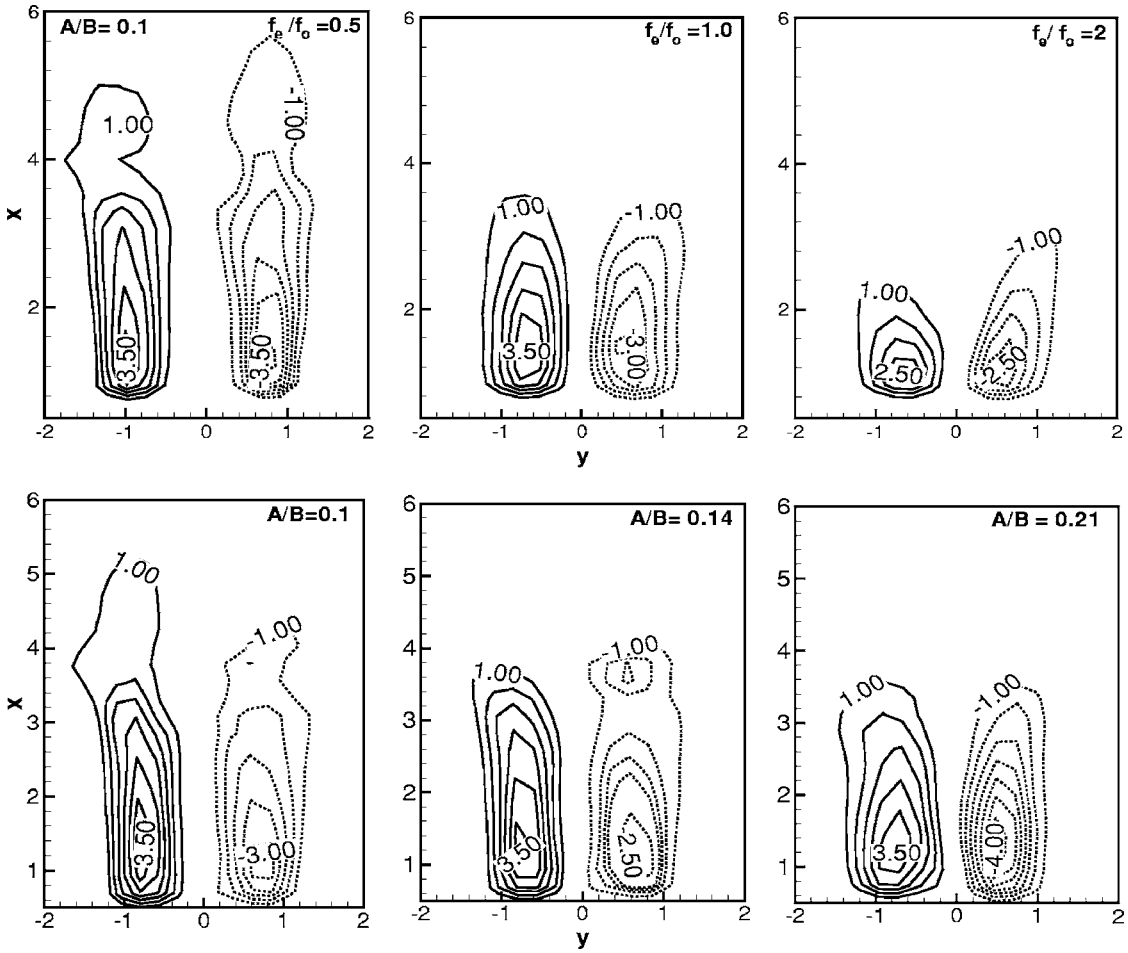

Fig. 19 Time-averaged spanwise vorticity contours (ω_z) for various forcing frequencies ($f/f_0=0.5,1,2$) (top) and amplitude ($A/B=0.1,0.14,0.21$) (bottom) at Re=170; aspect ratio=16

Acknowledgment

The authors acknowledge partial financial support received from the Naval Research Board, New Delhi, India, for this study.

Nomenclature

A = amplitude of oscillation, m
AR = aspect ratio, L/B
B = edge of the square cylinder, m
C_D = drag coefficient based on the average upstream velocity and B,
f = forcing frequency, Hz
f_o = vortex shedding frequency of stationary cylinder, Hz
KC = Carpenter number, $2\pi A/B$
L = length of the square cylinder, m
Re = Reynolds number based on cylinder diameter, $\rho UB/\mu$
rms = root-mean-square velocity, m/s
St = Strouhal number, fB/U
t = time
u = x component of velocity, m/s
U = upstream velocity, m/s
v = y component of velocity, m/s
V_r = reduced velocity, U/Bf
W = width of the test section, m
x,y,z = dimensionless coordinates from the cylinder center scaled by B

Greek symbols

μ = dynamic viscosity, kg/s m^2
ρ = density, kg/m^3
ω_z = spanwise component of the vorticity scaled by U/B

References

[1] Griffin, O. M., and Ramberg, S. E., 1976, "Vortex Shedding From a Cylinder Vibrating In-Line With an Incident Uniform Flow," J. Fluid Mech., **75**(2), pp. 257–271.
[2] Ongoren, A., and Rockwell, D., 1988, "Flow Structure From an Oscillating Cylinder Part 1. Mechanism of Phase Shift and Recovery in the Near Wake," J. Fluid Mech., **191**, pp. 197–223.
[3] Roussopoulos, K., 1993, "Feedback Control of Vortex Shedding at Low Reynolds Numbers," J. Fluid Mech., **248**, pp. 267–296.
[4] Gu, W., Chyu, C., and Rockwell, D., 1994, "Timing of Vortex Formation From an Oscillating Cylinder," Phys. Fluids, **6**(11), pp. 3677–3682.
[5] Tao, J. S., Huang, X. Y., and Chan, W. K. (1996), "A Flow Visualization Study on Feedback Control of Vortex Shedding From a Circular Cylinder," J. Fluids Struct., **10**, pp. 965–970.
[6] Krishnamoorthy, S., Price, S. J., and Paidoussis, M. P., 2001, "Cross-Flow Past an Oscillating Circular Cylinder: Synchronization Phenomena in the Near Wake," J. Fluids Struct., **15**, pp. 955–980.
[7] Cetiner, O., and Rockwell, D., 2001, "Streamwise Oscillations of a Cylinder in a Steady Current. Part 1. Locked-on States of Vortex Formation and Loading," J. Fluid Mech., **427**, pp. 1–28.
[8] Sarpkaya, T., 2004, "A Critical Review of the Intrinsic Nature of Vortex-Induced Vibrations," J. Fluids Struct., **19**, pp. 389–447.
[9] Yang, S. J., Cheng, T. R., and Fu, W. S., 2005, "Numerical Simulation of Flow Structures Around an Oscillating Rectangular Cylinder in a Channel Flow," Comput. Mech., **35**, pp. 342–351.
[10] Nobari, M. R. H., and Naderan, H., 2006, "Numerical Study of Flow Past a Cylinder With Cross Flow and Inline Oscillation," Comput. Fluids, **35**, pp. 393–415.
[11] Nishihara, T., Kaneko, S., and Watanabe, T., 2005, "Characteristics of Fluid Dynamic Forces Acting on a Circular Cylinder Oscillated in the Streamwise Direction and Its Wake Patterns," J. Fluids Struct., **20**, pp. 505–518.
[12] Westerweel, J., Dabiri, D., and Gharib, M., 1997, "The Effect of a Discrete Window Offset on the Accuracy of Cross-Correlation Analysis of PIV Recordings," Exp. Fluids, **23**, pp. 20–28.
[13] Chang, K.-A., and Liu, P. L.-F., 2000, "Pseudo Turbulence in PIV Breaking-Wave Measurements," Exp. Fluids, **29**, pp. 331–338.
[14] Keane, R. D., and Adrian, R. J., 1990, "Optimization of Particle Image Velocimeters. Part I: Double-Pulsed System," Meas. Sci. Technol., **1**, pp. 1202–1215.
[15] Konstantinidis, E., Balabani, S., and Yianneskis, M., 2003, "Effect of Flow Perturbations on the Near Wake Characteristics of a Circular Cylinder," J. Fluids Struct., **18**, pp. 367–386.
[16] Zdravkovich, M. M., 2003, *Flow Around Circular Cylinders*, Oxford University Press, London, Vol. 2.
[17] Williamson, C. H. K., and Roshko, A., 1988, "Vortex Formation in the Wake of an Oscillating Cylinder," J. Fluids Struct., **2**, pp. 355–381.
[18] Davis, R. W., and Moore, E. F., 1984, "A Numerical Study of Vortex Shedding From Rectangles," J. Fluid Mech., **116**, pp. 475–506.
[19] Sohankar, A., Norberg, C., and Davidson, L., 1999, "Simulation of Three-Dimensional Flow Around a Square Cylinder at Moderate Reynolds Numbers," Phys. Fluids, **11**(2), pp. 288–306.
[20] Saha, A. K., Muralidhar, K., and Biswas, G., 2003, "Investigation of Two and Three Dimensional Models of Transitional Flow Past a Square Cylinder," J. Eng. Mech., **129**(11), pp. 1320–1329.